Chapter 6

Determining Equilibrium Structures and Potential Energy Functions for Diatomic Molecules

Robert J. Le Roy

CONTENTS [1]

Because the Hamiltonian governing the vibration-rotation motion of diatomic molecules is essentially one dimensional, the theory is relatively tractable, and analyses of experimental data can be much more sophisticated than is possible for polyatomics. It is therefore possible to determine equilibrium structures to very high precision – up to 10^{-6} Å – and often also to determine accurate potential energy functions spanning the whole potential energy well. The traditional way of doing this involves first determining the v-dependence of the vibrational level energies G_v and inertial rotational constants B_v, and then using a semiclassical inversion procedure to

[1] **Chapter 6, pp. 159-203, of** *Equilibrium Structures of Molecules*, **J. Demaison and A. G. Csaszar editors, Taylor & Francis, London (2011).** Note that the pagination of this offprint is not identical to that in the published version of this chapter.

determine the potential energy function as an array of points. A more modern approach is to perform fully quantum mechanical 'direct potential fits', in which least-squares fits of transition energies to energy level differences computed from a parameterized analytic potential energy function are used to optimize the parameters defining that function. A key challenge of this approach is the determination of an optimal analytic potential function form. In both approaches, a combined-isotopologue data analysis allows one to account for Born-Oppenheimer breakdown effects.

6.0 Introduction

For diatomic molecules we are able to obtain a much broader range of information from experimental data than is possible for larger molecules. In addition to equilibrium structures, we can often determine an accurate bond dissociation energy, an accurate potential curve for the whole potential well, and sometimes also the Born-Oppenheimer breakdown radial strength functions which define the small differences between the electronic and centrifugal potential energy functions for different isotopologues of a given species. Such results allow us to make realistic predictions of the energies and properties of unobserved levels and of a wide range of other types of data not considered in the original data analysis, including collisional properties of the atoms produced on dissociating the molecular state of interest. All of this is possible for two reasons: the first is that modern experimental methods often provide very high quality data for vibrational levels spanning a large fraction of the potential well; the second is the fact that the relevant Schrödinger equation is effectively one-dimensional, and can be solved efficiently using standard numerical methods. The present chapter takes the first point for granted, and focuses on how the experimental information thus obtained can be used to determine both precise and accurate equilibrium properties, and reliable overall potential energy functions for diatomic molecules.

There are two basic approaches to the determination of diatomic molecule potential energy functions from experimental data. The first begins with a description of the patterns of molecular level energies as analytic functions (usually polynomials) of the vibrational and rotational quantum numbers, and uses an inversion procedure based on a semiclassical quantization condition to determine an extremely precise and smooth pointwise potential energy function. The second is fully quantum mechanical, and uses direct fits of simulated spectra to experimental data to determine parameters defining an analytic potential energy function. While the latter approach is better in principle, the associated fits are non-linear, and hence require realistic initial trial parameter values (see Chapter 2) which are most readily obtained from a preliminary analysis of the data using the conventional parameter-fit/semiclassical-inversion methodology (see § 6.2). This conventional approach also offers more direct insight regarding how various features of the data reflect the properties of the potential energy function, as well as insight regarding the nature and magnitude of isotope effects.

The following presentation begins in § 6.1 with a description of the 'forward' problem of calculating vibrational-rotational level energies and some spectroscopic properties from an assumed-known potential energy function. Section 6.2 then describes the 'traditional' semiclassical-based methods for the inverse problem of determining a potential energy function from experimental data, while the fully quantum mechanical 'direct-potential-fit' (DPF) procedure for determining potentials is described in § 6.3. Finally, the determination of Born-Oppenheimer breakdown (BOB) radial strength functions, which account for the differences between the potentials for different isotopologues and for some non-adiabatic couplings, are presented in § 6.4.

6.1 Quantum Mechanics of Vibration and Rotation

If we ignore Born-Oppenheimer breakdown and effects due to non-zero electronic and spin angular momentum, the vibration-rotation level energies of a diatomic molecule are the eigenvalues of the one-dimensional effective radial Schrödinger equation

$$-\frac{\hbar^2}{2\mu}\,\frac{d^2\,\psi(r)}{dr^2} \;+\; V_J(r)\;\psi(r) \;=\; E\,\psi(r) \quad , \tag{6.1}$$

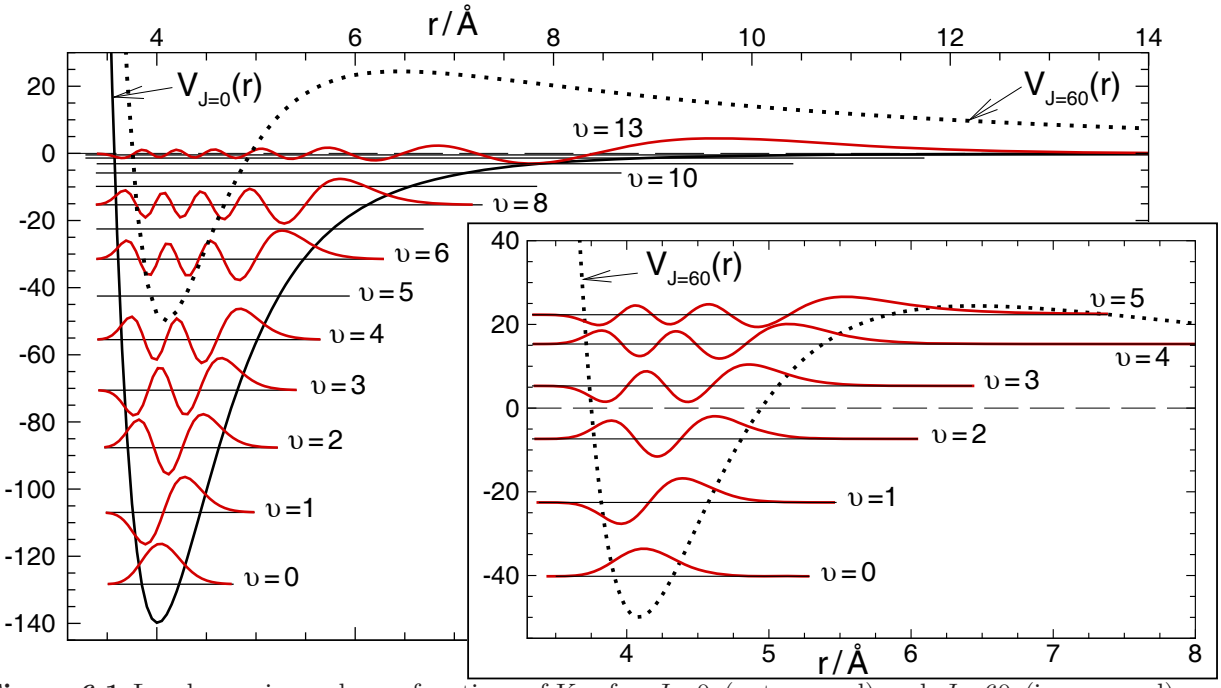

Figure 6.1 Level energies and wavefunctions of Kr_2 for $J=0$ (outer panel) and $J=60$ (inner panel).

in which r is the internuclear distance, $\hbar$ is Planck's constant divided by 2π, $\mu = m_A\, m_B/(m_A + m_B)$ is the reduced mass of the two atoms forming the molecule, and the overall effective potential energy function

$$V_J(r) \;=\; V(r) \;+\; \frac{\hbar^2}{2\mu\, r^2}\,[J(J+1)] \tag{6.2}$$

is the sum of the effective electronic potential $V(r)$ plus the centrifugal potential due to molecular rotation. If we ignore the effect of rotation, exact analytic solutions of Eq. (6.1) are known for a number of simple analytic potential energy functions, the most familiar of which are the particle-in-a-box square-well potential, the harmonic oscillator potential, $V_{\rm HO}(r) = \frac{1}{2}\,k(r-r_e)^2$, in which k is the quadratic force constant and r_e the equilibrium internuclear distance, and the Morse potential

$$V_{\rm M}(r) \;=\; \mathfrak{D}_e\left[1 - e^{-\beta(r-r_e)}\right]^2 \quad , \tag{6.3}$$

in which r_e is as defined above and $\mathfrak{D}_e$ is the well depth.

The eigenvalue expression for the particle-in-a-box, $E(v) = [h^2/(8\mu L^2)]\,(v+1)^2$, tells us that all else being equal, vibrational level spacings decrease when the width of the box L increases, or when the effective mass μ increases. The energy equation for a harmonic oscillator, $E(v) = \omega_e(v + {}^1\!/_2)$ with $\omega_e = \hbar\sqrt{k/\mu}$ then tells us that if the width of the potential is exactly proportional to the square root of the energy, the level spacings will be constant. Thus, if the well width increases more rapidly than the square root of the energy, the level spacings will *de*crease with increasing energy. More generally, this means that the pattern of vibrational level spacings reflects/determines the rate at which the width of the potential well increases with energy. Unfortunately, none of the simple analytic potentials for which closed-form solutions are known has sufficient flexibility and sophistication to describe accurately vibrational levels spanning a large fraction of the potential energy well of a real molecule. As a result, accurate treatments of real molecules necessarily depend on numerical methods.

For a realistic single-minimum potential energy function, Fig. 6.1 illustrates the pattern of vibrational levels, the nature of the vibrational wavefunctions, and shows how these properties are affected by molecular rotation. Because of potential function anharmonicity, the level spacings systematically decrease with increasing energy, and for the rotationless molecule (back panel), those spacing approach zero at the asymptote. This figure also illustrates the extreme asymmetry of the wavefunctions for levels approaching the dissociation limit. In particular, we see that for $v = 13$ the maximum in the probability amplitude lies

near 9.6 Å; for the highest level supported by this potential ($v = 15$) which is bound by only 0.0008 cm^{-1}, the outermost wavefunction maximum lies beyond 22 Å! This extreme wavefunction asymmetry can present challenges when eigenvalue calculations are being performed for levels lying very near the dissociation limit.

The dotted curves in both panels of Fig. 6.1 show the effective centrifugally distorted potential $V_J(r)$ for the case in which the angular momentum corresponds to $J = 60$, and the front panel shows the vibrational level energies and wavefunctions for this case. This emphasizes the important point that rotational level energies should not be thought of as a stack of sublevels associated with each pure vibrational ($J = 0$) level, but rather as vibrational levels of the centrifugally distorted potentials $V_J(r)$ for various J. This figure also shows that metastable 'quasibound' levels lying above the potential asymptote but below a potential barrier maximum have essentially the same qualitative properties as truly bound levels. In practice, most may be observed by sharp lines in experimental spectra, although the levels lying closest to a barrier maximum will be broadened by tunneling predissociation [1, 2, 3]. Figure 6.1 also shows that as J increases, the centrifugal potential will systematically spill vibrational levels out of the well until (at $J = 104$ for Kr_2) none remain.

In principle, a wide range of numerical methods may be used to solve Eq. (6.1) to virtually any desired precision. In practice, however, many methods are unable to routinely treat quasibound levels and bound levels lying very near dissociation as well as the more commonly considered deeply bound levels. While it is beyond the scope of this chapter to discuss such details, the author's strong preference is for a Cooley-type implementation of the Numerov wavefunction propagator method [4], since it may readily be combined with a third-turning-point boundary condition that allows quasibound levels to be located as easily as truly bound states [1, 2, 3]. A 'black box' computer code (accompanied by a manual) for determining any or all vibration-rotation eigenvalues and eigenfunctions of *any* plausible radial potential $V(r)$ is freely available on the www [3].

From a given set of calculated eigenvalues and eigenfunctions, it is a straightforward matter to use the wavefunctions to compute properties such as expectation values of powers of r or of the dipole moment or other functions of r, or to to calculate the matrix elements (overlap integrals) between different levels of a given potential or between levels of two different potential energy functions required for predicting transition intensities[3]. One can also use such 'forward' calculations to generate values of some conventional spectroscopic constants. In particular, it had long been customary to express the energies of rotational sublevels of a diatomic molecule in terms of a power series expansion about the rigid-rotor limit using the expression [5]:

$$E(v, J) \;=\; G_v + B_v[J(J+1)] - D_v[J(J+1)]^2 + H_v[J(J+1)]^3 + L_v[J(J+1)]^4 + \ldots \tag{6.4}$$

It had also long been known that if the centrifugal term in Eq. (6.2) is treated as a perturbation, first-order perturbation theory allows the inertial rotation constant for any given vibrational level v to be defined as [5]

$$B_v \;=\; \frac{\hbar^2}{2\mu} \left\langle \psi_v(r) \left| \frac{1}{r^2} \right| \psi_v(r) \right\rangle \quad . \tag{6.5}$$

Then in 1981 Hutson [6] showed that exact quantum mechanical values of the centrifugal distortion constants for all vibrational levels of a given potential well could be generated readily by solving inhomogeneous versions of Eq. (6.1) in which the inhomogeneous term depends on lower-order solutions and on the centrifugal term $\hbar^2/(2\mu r^2)$. This quickly became a standard procedure, and it is now a routine matter to calculate the "band constants" $\{G_v,\ B_v,\ D_v,\ H_v,\ \ldots\}$ associated with all vibrational levels of any given diatomic molecule potential [6, 7, 3].

It had also long been customary to express the vibrational level energies as expansions about the harmonic oscillator limit

$$G_v \;=\; \omega_e(v + 1/2) - \omega_e x_e(v + 1/2)^2 + \omega_e y_e(v + 1/2)^3 + \omega_e z_e(v + 1/2)^4 + \ldots \quad , \tag{6.6}$$

and analogous power series expansions in $(v + 1/2)$ are used to express the v-dependence of the various rotational constants B_v, D_v, H_v, ... , etc. [5]. Consideration of the expression for the inertial rotational constant

$$B_v \;=\; B_e - \alpha_e(v + 1/2) + \gamma_e(v + 1/2)^2 + \ldots \quad , \tag{6.7}$$

together with Eq. (6.5) indicates that within the approximation that the potential minimum corresponds to $v = -1/2$, the expression

$$r_e \;\approx\; r_e^{(1)} \;=\; \sqrt{\hbar^2/(2\mu\, B_e)} \tag{6.8}$$

yields a good first-order estimate of the equilibrium structure. Unfortunately, although $v=-1/2$ corresponds to the potential minimum both for the quantum mechanical harmonic and Morse oscillators, and for all other potentials within the first-order semiclassical approximation (see § 6.2.1), it is not precisely true for real molecules. Hence, use of this simple extrapolation of an empirical B_v function to obtain an estimate of the equilibrium bond length requires small corrections (see § 6.2.1).

For the case of a potential function expressed as a harmonic oscillator with higher-order power-series terms treated as corrections, Kilpatrick and Kilpatrick used perturbation theory to show that power series in $(v + 1/2)$ are indeed a natural way of expressing the v–dependence of the various band constants of Eq. (6.4) [8, 9]. However, the resulting expressions quickly grow to have an intimidating degree of complexity, and hence do not provide a practical way of defining unique values of parameters such as ω_e, $\omega_e x_e$, $\omega_e y_e$, ... , etc., associated with a given potential energy function. This remains true today, and in practice, except for the very lowest-order terms, the $(v + 1/2)$ expansion coefficients associated with the band constants for a given potential energy function can only be obtained from empirical fits to calculated values of those band constants.

The perturbation-theory expressions of Kilpatrick and Kilpatrick [8, 9] proved difficult to work with and impractical to invert. The absence of any other fully quantum mechanical technique for inverting discrete spectroscopic data to obtain potential energy functions stimulated the development and very wide application of methods based on approximate semiclassical procedures for solving the radial Schrödinger equation. Although these semiclassical methods are not as accurate as a full quantum treatment, their robustness and ease of use made them the basis for most practical diatomic molecule spectroscopic data analyses for more than half a century.

6.2 Semiclassical Methods

6.2.1 The Semiclassical Quantization Condition

Semiclassical or "phase integral" methods are approximate techniques for solving differential equations that were well known to mathematicians in the nineteenth century. They were well developed in the early days of quantum mechanics, and while they are approximate, they often provide quite accurate results, particularly for species whose reduced masses are relatively large. The tractability of semiclassical methods also made them particularly useful prior to the improvements in digital computers that have made applications of the modern fitting/inversion methods of § 6.3 feasible. Moreover, the explicit expressions that they yield for relating patterns of level energies to the nature of the potential energy function provide an important source of physical insight. Indeed, semiclassical theory is the basis for much of our understanding of isotope effects in molecular spectra, as well as for some of the most widely used data inversion methods in molecular physics [10, 11].

The semiclassical approach to solving the one-dimensional radial Schrödinger equation Eq. (6.1) begins by writing the eigenfunction in the form

$$\psi(r) \;=\; e^{i\,\mathcal{S}(r)/\hbar} \quad , \tag{6.9}$$

in which $i \equiv (-1)^{1/2}$. Substituting this expression into Eq. (6.1) and removing the common factor $e^{i\mathcal{S}(r)/\hbar}$ yields a differential equation for $\mathcal{S}(r)$ which is precisely equivalent to the original Schrödinger equation:

$$i\hbar\,\frac{d^2\,\mathcal{S}}{dr^2} \;-\; \left(\frac{d\mathcal{S}}{dr}\right)^2 \;+\; 2\mu\,[E - V_J(r)] \;=\; 0 \quad . \tag{6.10}$$

Since Planck's constant $\hbar$ is quite small, the first term in this differential equation will be much smaller than the second, so a reasonable zero'th-order approximation (partly corrected for later) is to neglect it, yielding a simple first-order equation whose solution is

$$S^{(0)}(r) \;=\; \pm\,\hbar \int^r Q(r')\,dr' \quad , \tag{6.11}$$

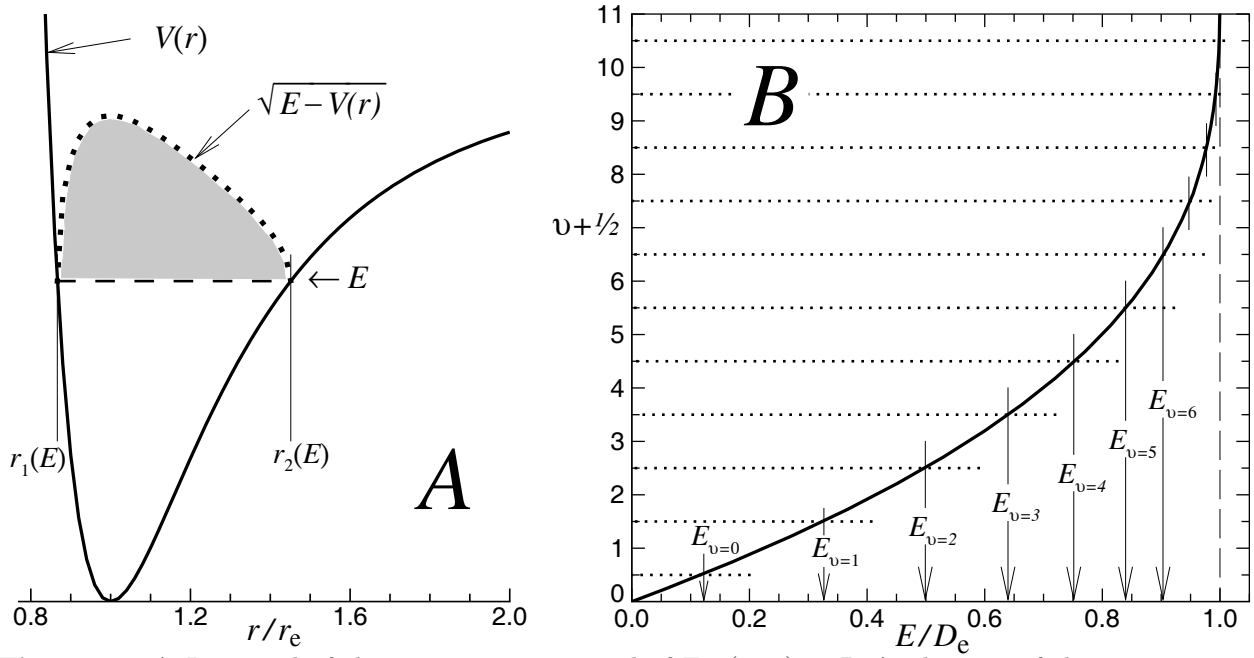

Figure 6.2 *A*. Integrand of the quantization integral of Eq. (6.13). *B*. Application of the quantization condition of Eq. (6.13) for defining first-order semiclassical eigenvalues.

in which $Q(r') \equiv \sqrt{(2\mu/\hbar^2)[E - V_J(r')]}$. Using the second derivative of this result to replace the first term in Eq. (6.10) then yields an improved first-order differential equation for $\mathcal{S}(r)$ whose solution yields the "first-order" semiclassical approximation for the wavefunction:

$$\psi^{(1)}(r) \;=\; \frac{A}{\sqrt{|Q(r)|}} \;\exp\!\left\{\pm i \int^{r} Q(r')\,dr'\right\} \quad . \tag{6.12}$$

Equation (6.12) is a fairly good approximation for the wavefunction except near classical turning points, where $Q(r)=0$ (e.g., near the points $r_1(E)$ and $r_2(E)$ in Fig. 6.2 *A*). However, in the immediate neighbourhood of such turning points it is a very good approximation to represent the potential as a linear function of r. The exact solutions of the Schrödinger equation for a linear potential are Airy functions, whose properties are well known [12]. The combination of Airy functions near the turning points with the semiclassical wavefunctions of Eq. (6.12) in other regions then provides a reasonably good representation for the wavefunction at all distances.

Finally, one can show that the usual boundary conditions that the wavefunction must die off in the classically forbidden regions where $E < V_J(r)$ are only satisfied if the integral of $Q(r)$ over the classically allowed region between the inner and outer turning points $r_1(E)$ and $r_2(E)$ (see Fig. 6.2 *A*) is precisely equal to a half-integer multiple of π [11]. In other words, the eigenvalues of the given potential are the discrete energies for which

$$v + {}^1\!/_2 \;=\; \frac{1}{\pi}\sqrt{\frac{2\mu}{\hbar^2}} \int_{r_1(E)}^{r_2(E)} [E - V_J(r)]^{1/2}\,dr \quad , \tag{6.13}$$

with v being the (integer) vibrational quantum number of the level in question. This expression is known as the Bohr-Sommerfeld quantization condition.

Panel *A* of Fig. 6.2 illustrates the definition of the inner and outer turning points $r_1(E)$ and $r_2(E)$ of a potential energy curve $V(r)$ at a given energy E, and the shaded area shows the integrand of the integral of Eq. (6.13). Panel *B* then shows how the right-hand side of Eq. (6.13) varies as the energy increases from the potential minimum to the dissociation limit of a typical single-minimum potential. Within the first-order semiclassical approximation, the energies at which the dotted horizontal lines at half-integer values of $(v+{}^1\!/_2)$ intersect this curve define the discrete vibrational level energies of this potential.

Because it is based only on the first-order semiclassical wavefunction of Eq. (6.12), the quantization con-

dition of Eq. (6.13) lacks full quantum mechanical accuracy, and as a result it is rarely used for practical eigenvalue calculations. However, its simple form and explicit dependence on the potential energy function means that for certain types of analytic potentials it may be inverted to give explicit expressions for vibrational-rotational level energies as functions of the parameters defining the potential. Moreover, we shall see that this quantization condition can also be inverted to yield a numerical procedure for calculating a pointwise potential function from a knowledge of experimental vibration-rotation level spacings.

The most famous and most widely used potential for which analytic level-energy expressions may be obtained from Eq. (6.13) is a 'Dunham-type' potential, which is a polynomial expansion about the equilibrium internuclear distance:

$$V_{\rm Dun}(r) \;=\; a_0\,\xi^2\left(1 + a_1\,\xi + a_2\,\xi^2 + a_3\,\xi^3 + \ldots\right) \quad , \tag{6.14}$$

in which $\xi \equiv (r - r_e)/r_e$ is the relative displacement from equilibrium. Since $r = r_e(1+\xi)$, the centrifugal potential may also be expressed as a power series in ξ:

$$\frac{[J(J+1)]\,\hbar^2}{2\mu\,r^2} \;=\; \frac{[J(J+1)]\,\hbar^2}{2\mu(r_e)^2}\;\left\{1 - 2\xi + 3\xi^2 - 4\xi^3 + \ldots\right\} \quad , \tag{6.15}$$

so that the overall potential $V_J(r)$ may also be written as a power series in ξ. In 1932 Dunham showed that upon substituting such a polynomial potential into the quantization condition of Eq. (6.13) and applying some clever manipulations, an explicit power-series expression for the level energies may be obtained,

$$E(v,J) \;=\; \sum_{m=0}\sum_{\ell=1} Y_{\ell,m}\,(v + {}^1\!/_2)^\ell\,[J(J+1)]^m \quad , \tag{6.16}$$

whose coefficients $Y_{\ell,m}$ are explicitly known functions of the potential parameters $\{a_0,\, a_1,\, a_2,\, a_3,\, \ldots\}$ [13]. His derivation showed that this double power series in $(v + {}^1\!/_2)$ and $[J(J+1)]$ was indeed a natural way to describe level energies [13]. However, until relatively recently (see § 6.3), the complexity of the algebraic expressions for the higher-order $Y_{\ell,m}$ coefficients, and the even greater complexity arising if a more accurate higher-order version of the quantization condition is utilized, discouraged practical use of Dunham-type expressions for determining potential energy functions.

While the above discussion considered only the first-order semiclassical approximation, extended versions of Eq. (6.13) have been derived based on third-order, fifth-order, and even higher-order semiclassical approximations for the wavefunctions [14]. In particular, the third-order quantization condition has the form

$$v + {}^1\!/_2 \;=\; \frac{1}{2\pi}\sqrt{\frac{2\mu}{\hbar^2}}\oint [E - V_J(r)]^{1/2}\,dr \;+\; \frac{1}{96\pi}\sqrt{\frac{\hbar^2}{2\mu}}\;\oint \frac{V''(r)}{[E - V_J(r)]^{3/2}}\;dr \quad , \tag{6.17}$$

in which line integrals have been replaced by contour integrals. The additional power of $\hbar^2$ associated with each higher order of approximation tells us that the accuracy of such treatments quickly approaches that of the full quantum result [15, 16].

Dunham's original derivation included some consideration of this leading higher-order correction term [13], and the resulting estimate of the value of this term at the potential minimum ($E = 0$) led to an improved estimate for the value of v associated with the potential minimum [5]:

$$v_{\rm min} \;=\; -\,{}^1\!/_2 \;-\; \delta v_{\rm min} \;=\; -\,{}^1\!/_2 \;-\; \left\{\frac{B_e - \omega_e x_e}{4\,\omega_e} \;+\; \frac{\alpha_e}{12\,B_e} \;+\; \frac{\omega_e}{B_e}\left(\frac{\alpha_e}{12\,B_e}\right)^2\right\} \quad . \tag{6.18}$$

This result in turn allows an improved 'third-order semiclassical' estimate of the equilibrium bond length to be obtained from the empirical knowledge of the v–dependence of the vibrational energies and inertial rotation constants represented by Eqs. (6.6) and (6.7):

$$r_e \;=\; r_e^{(3)} \;=\; \sqrt{\hbar^2/(2\mu\,B_{v=v_{\rm min}})} \quad . \tag{6.19}$$

Use of Eq. (6.19) provides the best estimate of a diatomic molecule equilibrium bond length that can be extracted from the conventional empirical expressions for vibrational-rotational level energies, namely,

Eqs. (6.4), (6.6) and (6.7). The methodologies described in § 6.3 provide an alternate, and arguably more direct, way of determining such equilibrium bond lengths. However, it is important to remember that the existence of quantum-mechanical zero-point energy means that this equilibrium distance does not describe the actual effective bond length of any real molecule. A best estimate for that distance would be the average bond length of the molecule in its ground vibration-rotation level,

$$\overline{r}_{0,0} \;=\; \langle \psi_{0,0}(r) | r | \psi_{0,0}(r) \rangle \quad , \tag{6.20}$$

in which $\psi_{v,J}(r)$ is the radial wavefunction in vibration-rotation state (v, J). However, there is no direct empirical way of determining this quantity, and to calculate it requires a knowledge of the potential energy function that would allow the radial wavefunction for the zero-point level to be determined. This result indicates that determination of precise values for real diatomic molecule bond lengths cannot be achieved simply from manipulation of empirical molecular constants, but also requires a knowledge of the potential energy function.

In closing this subsection, it is important to note that the real ground-state bond length $\overline{r}_{0,0}$ usually differs significantly both from r_e and from the average bond length implied by the inertial rotational constant for the ground vibrational level, $\langle r^{-2} \rangle^{-1/2} = \sqrt{\hbar^2/(2\mu\, B_{v=0})}$. For example, for the ground electronic state of H_2: $\overline{r}_{0,0} = 1.034\, r_e = 1.021\, \langle r^{-2} \rangle^{-1/2}$ [17]. The large differences between these three quantities provides a sober warning about the danger of thinking of the type of average bond length obtained from an empirical inertial rotation constants B_v as being the actual average bond length for a molecule in a given vibrational level.

6.2.2 The Rydberg-Klein-Rees (RKR) Inversion Procedure

By 1929, even before Dunham's landmark papers, the drawbacks of trying to work with model potentials for which exact analytic quantum mechanical eigenvalue solutions existed were becoming evident, since the few such functions available were not flexible enough to account fully for experimental data spanning a significant fraction of a potential well. As a result, researchers began to investigate the use of semiclassical methods. A key pioneer in this area was Oldenberg, who noticed that according to Eq. (6.13), the rate at which v changed with vibrational energy E_v depended on the rate at which the width of the potential well increased with energy [18]. Another pioneer was Rydberg, who noticed that the concomitant change in the inertial rotational constant B_v placed a constraint on the asymmetry of that rate of growth [19].

A formal derivation based on these observations was reported by Klein in 1932 [20]. He began by taking the derivative of Eq. (6.13) with respect to the vibrational energy, and then broke the integral into two segments to obtain

$$\frac{dv}{dE} \;=\; \frac{1}{2\pi} \sqrt{\frac{2\mu}{\hbar^2}} \left\{ \int_{r_1(E)}^{r_e} \frac{dr}{[E - V(r)]^{1/2}} \;+\; \int_{r_e}^{r_2(E)} \frac{dr}{[E - V(r)]^{1/2}} \right\} \quad . \tag{6.21}$$

Replacement of the integration over r by an integration over values of the potential energy with increment du then yielded the expression

$$\frac{dv}{dE} \;=\; \frac{1}{2\pi} \sqrt{\frac{2\mu}{\hbar^2}} \int_0^E \left\{ \frac{dr_2(u)}{du} \;-\; \frac{dr_1(u)}{du} \right\} \frac{du}{[E - u]^{1/2}} \quad . \tag{6.22}$$

The next steps consisted of replacing E in the above expression by E', multiplying both sides by the factor $dE'/[E - E']^{1/2}$, interchanging the order of the resulting double integration on the right hand side, and then integrating both sides over the variable E' from its minimum (the current value of u) to E while making use of the mathematical identity

$$\int_u^E \frac{dE'}{\sqrt{(E - E')(E' - u)}} \;=\; \pi \quad . \tag{6.23}$$

When this was done, the remaining integral on the right hand side of the equation collapsed to the difference $r_2(E) - r_1(E)$. Finally, replacement of the integration over u by an integration over the vibrational quantum

number v' yielded the first of the 'RKR' equations:

$$r_2(v) \; - \; r_1(v) \; = \; 2\sqrt{\frac{\hbar^2}{2\mu}} \; \int_{-1/2}^{v} \; \frac{dv'}{[G_v - G_{v'}]^{1/2}} \; \equiv \; 2\,f \quad . \tag{6.24}$$

In this final result the notation for the energy E has been replaced by the symbol G_v normally employed for vibrational energy, and use has been made of the fact that within the first-order quantization condition of Eq. (6.13), the potential minimum corresponds to $v' = -1/2$.

The derivation of the second RKR equation begins by taking the partial derivative of Eq. (6.13) with respect to the factor $[J(J+1)]$ that defines the strength of the centrifugal contribution to the potential, and then setting $J = 0$:

$$\begin{aligned} \left(\frac{\partial v}{\partial [J(J+1)]}\right)_E \; &= \; \left(\frac{\partial v}{\partial E}\right)_J \; \left(\frac{\partial E}{\partial [J(J+1)]}\right)_v \; = \; B_v \left(\frac{\partial v}{\partial E}\right)_{J=0} \\ &= \; -\frac{1}{2\pi} \sqrt{\frac{2\mu}{\hbar^2}} \int_{r_1(E)}^{r_2(E)} \frac{dr}{r^2\,[E - V(r)]^{1/2}} \quad . \end{aligned} \tag{6.25}$$

Breaking the range of integration in two at r_e and applying the same manipulations described above then yields the second RKR equation,

$$\frac{1}{r_1(v)} \; - \; \frac{1}{r_2(v)} \quad = \quad 2\sqrt{\frac{2\mu}{\hbar^2}} \int_{-1/2}^{v} \; \frac{B_{v'}\; dv'}{[G_v - G_{v'}]^{1/2}} \; \equiv \; 2\,g \quad . \tag{6.26}$$

Combining Eqs. (6.24) and (6.26) then yields the final expressions for the turning points

$$r_2(v) \; = \; \left(f^2 \; + \; f/g\right)^{1/2} \; + \; f \tag{6.27}$$

$$r_1(v) \; = \; \left(f^2 \; + \; f/g\right)^{1/2} \; - \; f \quad . \tag{6.28}$$

In spite of their elegance and obvious potential utility, Klein's equations saw little practical use for over three decades. One reason for this would have been the practical difficulty of evaluating the Klein integrals accurately prior to the advent of digital computers. The nature of this problem is illustrated by the plots for the ground electronic state of Ca_2 shown in Fig. 6.3. Panels A and B show the nature of the $G_{v'}$ and $B_{v'}$ functions, while Panel C shows the integrands of Eqs. (6.24) and (6.26) for a representative vibrational level, $v = 26$. Although the areas under these curves are finite, the fact that the integrands go to infinity at the upper bound makes an accurate evaluation of these integrals somewhat challenging.

In 1947 Rees pointed out that the two Klein integrals could be evaluated in closed form if $G(v)$ and B_v were represented by sets of quadratic polynomials in v for different segments of the range of integration [21]. This contribution led to his name being attached to the method, but the inconvenience of having to fit data piecewise to sets of quadratics meant that it still saw little use. Finally, by the early 1960's a number of groups had developed computer programs for evaluating these integrals for any user-selected expressions for $G(v)$ and B_v, and the 'RKR' method quickly grew to become ubiquitously associated with diatomic molecule data analyses. However, truly efficient techniques for evaluating the Klein integrals which take proper account of the singularities in the integrand were not reported until 1972 [22, 23, 24].

One technique for evaluating the RKR integrals accurately is simply to introduce a transformation that removes the singularities. For example, introduction of the auxiliary variable $y = \sqrt{v - v'}$ transforms Eqs. (6.24) and (6.26) into the forms

$$r_2(v) \; - \; r_1(v) \quad = \quad 4\sqrt{\frac{\hbar^2}{2\mu}} \; \int_0^{\sqrt{v+1/2}} \left\{ \sqrt{\frac{v - v'}{G_v - G_{v'}}} \right\} dy \; = \; 2\,f \tag{6.29}$$

$$\frac{1}{r_1(v)} \; - \; \frac{1}{r_2(v)} \quad = \quad 4\sqrt{\frac{2\mu}{\hbar^2}} \int_0^{\sqrt{v+1/2}} \left\{ B_{v'} \sqrt{\frac{v - v'}{G_v - G_{v'}}} \right\} dy \; = \; 2\,g \quad . \tag{6.30}$$

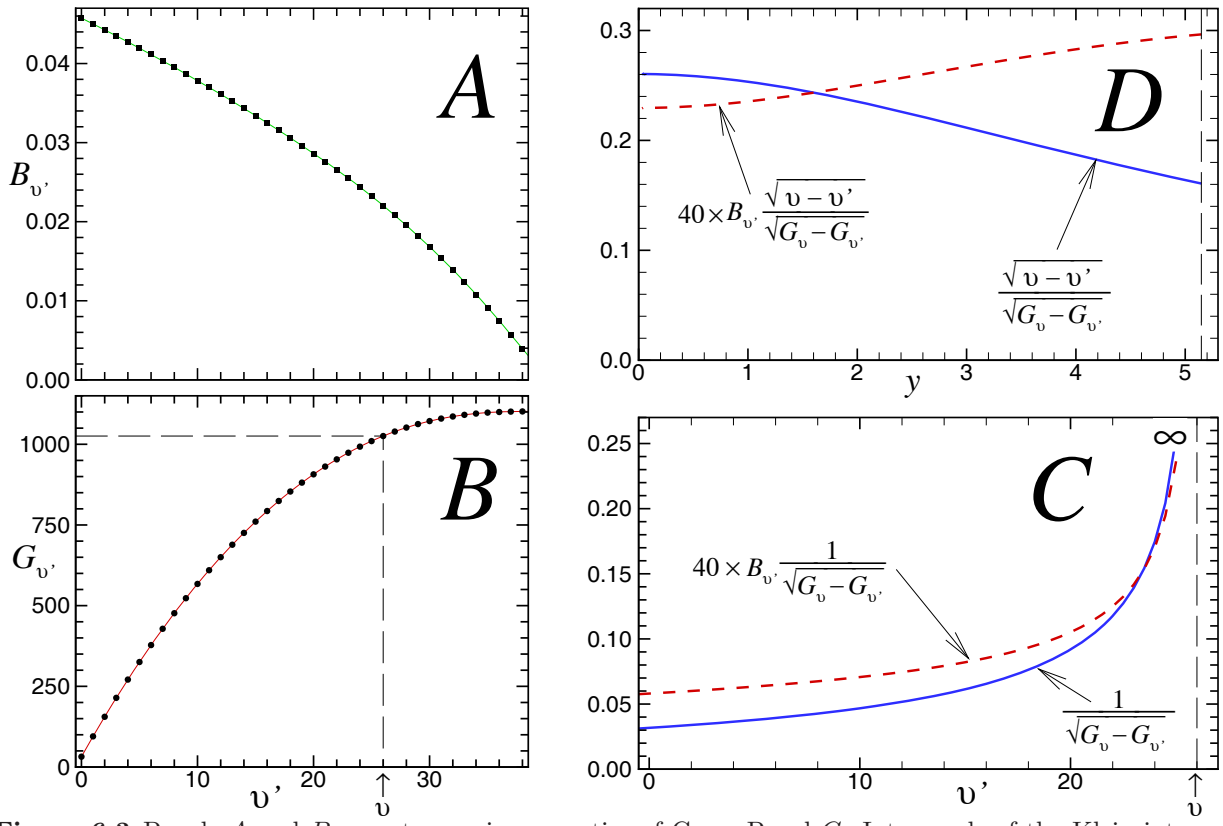

Figure 6.3 Panels A and B: spectroscopic properties of Ca_2. Panel C: Integrands of the Klein integrals of Eqs. (6.24) and (6.26) for level $v=26$ of Ca_2; a numerical factor of 40 has been introduced in order to place the two integrands on the same vertical scale. Panel D: Integrands of the transformed Klein integrals of Eqs. (6.29) and (6.30) for the case considered in Panel C. Units for energy are cm^{-1} in all panels.

As is illustrated by Panel D of Fig. 6.3, the integrands in these expressions are smooth and well behaved and have no singularities(!), so a very modest amount of computational effort can yield turning points converged to machine precision. A particularly convenient procedure is to apply a simple N–point Gauss-Legendre quadrature procedure to the whole interval, and then bisect that interval and apply the same procedure to both halves. At each such stage of subdivision the error will decrease by a factor of $1/2^{N-2}$ [12]; for $N=12$ this means an error reduction by three orders of magnitude at each stage of bisection.

It is important to remember that although the experimental data are only associated with integer values of v, the vibrational energies G_v and rotational constants B_v in these integrals must be treated as continuous functions of v. Moreover, as illustrated by Fig. 6.2 B, the quantization integral of Eq. (6.13) may be evaluated for *any* energy E (or G_v), independent of whether or not it corresponds to an integer value of v. Thus, we are free to solve the RKR equations and evaluate turning points for any chosen mesh of integer or non-integer v values. This is quite important, since solving the Schrödinger equation numerically requires an interpolation procedure to provide a mesh of accurate potential function values at distances that will not correspond to calculated turning points. If the evaluation procedure were restricted to turning points at integer v, such interpolations would often have limited accuracy, in spite of the fact that the calculated turning points would be smooth to machine precision.

Two other practical considerations intrude upon the use of RKR potentials. One is the perhaps obvious, but sometimes overlooked point that calculated turning points cannot really be trusted beyond the vibrational range of the experimental data used to determine the G_v and B_v functions. This restriction is partially lifted if 'near-dissociation expansions' of the type described in § 6.2.3 are used to represent G_v and B_v. However, use of the resulting potential to generate reliable solutions to the radial Schrödinger equation would still require functions for extrapolating inward and outward to be attached smoothly at the ends of the range of

calculated turning points.

The second practical concern arises from the fact that shortcomings of the experimentally-derived functions characterizing G_v and B_v will give rise to errors in calculated RKR turning points. Since the repulsive inner wall of a potential function is very steep, especially at high energies, such errors often manifest themselves as non-physical behaviour of the inner wall of the potential. For example, rather than have a (negative) slope and positive curvature that vary slowly with energy, the inner wall might pass through an inflection point and take on negative curvature, or it might turn outward with increasing energy, with the slope becoming positive. In practice, the experimental G_v function is usually defined with greater relative accuracy than is the B_v function. However, whatever the source of the problem, a modest degree of inappropriate behaviour of either the G_v or B_v function can give rise to non-physical behaviour of the inner wall of the potential, as the expected monotonic increase in slope with energy will greatly amplify the effect of even very small errors in the f and/or g integrals. Thus, the behaviour of the inner wall of any calculated RKR potential should always be examined, and if the slope deviates from smooth behaviour with positive curvature, it should be smoothed or replaced with a physically sensible extrapolating function.

Although small relative errors in the f or g integral can make the curvature or slope of the high-energy inner wall change in an unacceptable non-physical manner, the rapid growth of the f integral with increasing G_v means that the width of the potential $[r_2(v) - r_1(v)]$ as a function of energy may still be relatively well defined by Eq. (6.24) or (6.29), even when the directly calculated inner potential wall is unreliable. In this case, combining this directly-calculated well-width function with a reasonable extrapolated inner potential wall would yield a 'best' estimate of the upper portion of the potential (a procedure first introduced by Verma [25]). Similarly, even in the complete absence of rotational data, a combination of the well-width information yielded by the calculated f integrals with an inner wall defined by a model such as a Morse potential can give a realistic overall potential function [26]. A 'black box' computer code (accompanied by a manual) for performing RKR calculations, which allows the use of a variety of possible expressions for G_v and B_v and takes account of the practical concerns described above, is available on the www [27].

Finally, it is also important to remember that the manipulations of Eq. (6.13) to obtain the RKR equations (6.24) and (6.26) (or equivalently, (6.29) and (6.30)) are mathematically exact! In other words, within the first-order semiclassical or WKB approximation [11], this method yields a unique potential energy function which *exactly* reflects the input functions representing the v-dependence of the vibrational energy G_v and inertial rotational constant B_v. A nagging weakness, however, is the fact that the quantization condition of Eq. (6.13) is *not* exact, so quantum mechanical properties of an RKR potential will not agree precisely with the input G_v and B_v data used to generate that potential.

Table 6.1 illustrates this point for four species for which accurate and extensive G_v and B_v functions are available from the literature. Those functions were used to generate RKR potentials, after which an exact quantum procedure [3] was used to calculate the associated vibrational level spacings ($\Delta G_{v+1/2}$) and inertial rotational constants (B_v). The two final columns of this table show the root mean square differences between those calculated quantities and the values implied by the G_v and B_v functions used to generate the original RKR potential. In each case the range considered was truncated at $G(v_{\max})$ which is the smaller of the upper end to the range of the experimental data used to determine the G_v and B_v functions, or the point at which the onset of irregular behaviour of the inner-wall turning points (see above) required smoothing and inward extrapolation to be applied.

Table 6.1 Root mean square errors in vibrational level spacings and rotational constants calculated from RKR potentials for selected molecules.

molecule	μ	$\mathfrak{D}_e$ $[\mathrm{cm}^{-1}]$	$v_{\max}$	$\frac{G(v_{\max})}{\mathfrak{D}_e}$	$\mathrm{err}\{\Delta G_{v+1/2}\}$ $[\mathrm{cm}^{-1}]$	% $\mathrm{err}\{B_v\}$
BeH	0.906	17590	9	0.895	0.527	0.031
N_2	7.002	79845	20	0.529	0.052	0.0026
Ca_2	19.981	1102	25	0.9997	0.00079	0.0021
Rb_2	42.456	3993	85	0.916	0.00017	0.0013

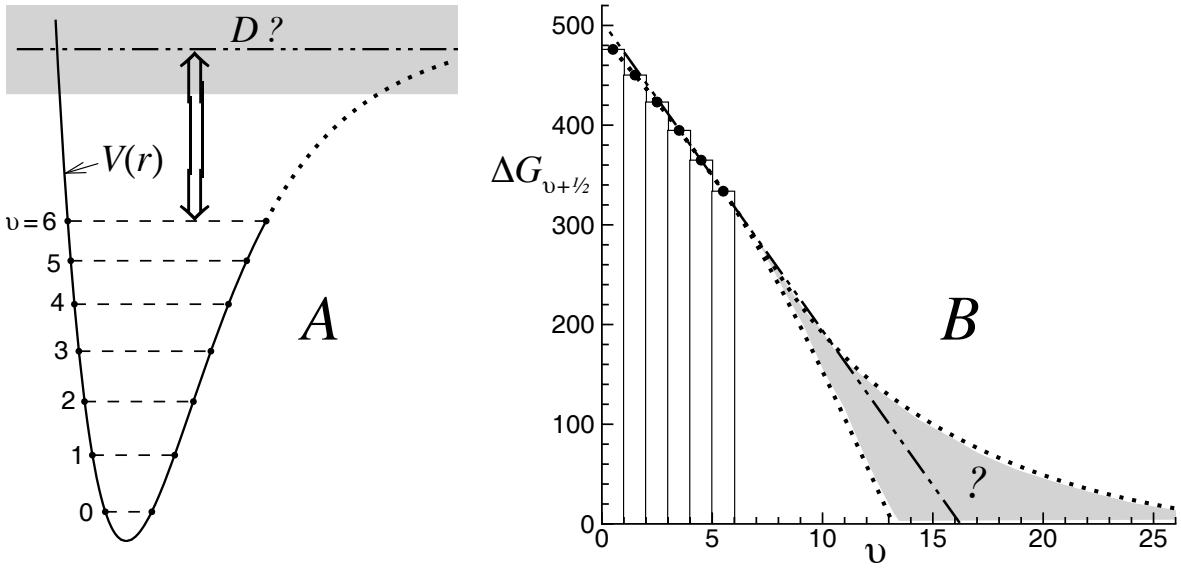

Figure 6.4 Panel *A*: Schematic illustration of the extrapolation problem of determining the dissociation limit $\mathfrak{D}$. Panel *B*: A Birge-Sponer plot in which the shaded area illustrates the uncertainty associated with conventional vibrational extrapolation.

These results show that errors in RKR potentials due to neglect of the second term in Eq. (6.17) are largest for species with small reduced mass. For a hydride they are quite significant, but their importance drops rapidly with increasing reduced mass, and for $\mu \gtrsim 20\,u$ (Ca_2 and Rb_2) the vibrational spacing discrepancies are smaller than typical experimental vibrational energy uncertainties. However, such discrepancies add up, and even for these 'heavy' species the accumulated error in the vibrational energy can be significant. Overall, although the situation is less satisfactory for light molecules, the first-order semiclassical nature of the RKR procedure has only a modest negative effect on the quality of the resulting potential, or of quantities calculated from it. At the same time, that fact that RKR potentials are defined as sets of many-digit turning points, often need to have their inner wall smoothed, and always need extrapolation functions attached at their inner and outer ends, are persistent inconveniences. These problems are resolved, however, by use of the methodology described in § 6.3.

In closing this discussion, it is worth noting that the RKR method itself provides no new information about equilibrium structures beyond that implicit in the first-order semiclassical result of Eq. (6.8). Although the higher-order quantization condition of Eq. (6.17) is not amenable to the exact inversion procedures described above, it has been suggested that better-than-first-order results could be obtained simply by replacing the lower bound on the integrals of Eqs. (6.24) and (6.26) by $v_{\min} = -1/2 - \delta v_{\min}$ from Eq. (6.18) [28]. Unfortunately, tests analogous to those of Table 6.1 show that although this procedure does give somewhat better results near the potential minimum, the discrepancies at higher v are larger than those obtained with the usual first-order method.

6.2.3 Near-Dissociation Theory (NDT)

The preceding discussion shows that the RKR method can give a quite accurate potential energy functions spanning the range of vibrational energies for which experimental data are available. However, it offers no advice regarding how to address the question illustrated in Panel *A* of Fig. 6.4: that is, how to estimate the distance from the highest observed vibrational level to the dissociation limit $\mathfrak{D}$, and how to estimate the number, energies, and other properties of levels lying above that highest observed vibrational level.

Panel *B* of Fig. 6.4 illustrates a graphical means for addressing this question which was introduced by Birge and Sponer in 1926 [29] and remained the method of choice for most of the following half century. In a Birge-Sponer plot the vibrational level spacings $\Delta G_{v+1/2} \equiv G_{v+1} - G_v$ are plotted against the vibrational quantum number, with the points placed at half-integer values of the abscissa. On this diagram, the numerical $\Delta G_{v+1/2}$ value is equal to the area of the narrow vertical rectangle whose upper edge is centred at that point.

As a result, the sum of the areas of the six illustrated rectangles is equal to the sum of the six $\Delta G_{v+1/2}$ values, which is, of course, the distance from level $v=0$ to level $v=6$. It is immediately clear that the area under a smooth curve through these points from $v=0$ to 6 is a very good approximation to that energy difference. Birge and Sponer then pointed out that if this curve was extrapolated to cut the v axis, the area under the curve in the extrapolation region would be a very good approximation to the distance from the highest observed level to the dissociation limit. Moreover, the points at which the extrapolated curve crossed half-integer v value gives predicted vibrational spacings for unobserved levels extending all the way to the limit. If these predictions were correct, an RKR potential based on the resulting extrapolated G_v values could be calculated for the whole well.

The only problem with Birge-Sponer plots is the uncertainty regarding how to perform the extrapolation, a problem which remained an open question for 44 years. The dash-dot-dot line on Fig. 6.4 *B* shows a linear extrapolation through the last two experimental points, while the dotted curves bounding the shaded region are plausible alternative extrapolations, one with negative and one with positive curvature. The ratio of the area of the shaded region to the overall area under the curve in the extrapolation region is then an indication of the relative uncertainty in the distance from the last observed level to the dissociation limit. Unfortunately, it is clear that this uncertainty could be as large as 50-100%!

A solution to this extrapolation problem was finally reported in 1970 [30]. It was based on the realization that another type of potential for which an explicit analytic expression for the vibrational level energies may be obtained from Eq. (6.13) is the attractive inverse-power function $V(r)=\mathfrak{D}-C_n/r^n$ whose form matches the limiting long-range behaviour of all intermolecular interactions. As was true for the RKR method, the derivation is remarkably straightforward.

Since the nature of *distribution* of vibrational levels near dissociation is being sought, the derivation begins by taking the derivative of Eq. (6.13) with respect to the vibrational level energy to obtain an expression for the density of states at energy G_v (for $J=0$):

$$\frac{dv}{dG_v} \;=\; \frac{1}{2\pi}\,\sqrt{\frac{2\mu}{\hbar^2}}\,\int_{r_1(v)}^{r_2(v)} \frac{dr}{[G_v - V(r)]^{1/2}} \quad . \tag{6.31}$$

Consider now the nature of the integrand appearing in Eq. (6.31). For a model Lennard-Jones(12,6) potential function

$$V_{\rm LJ}(r) \;=\; \frac{C_{12}}{r^{12}} \;-\; \frac{C_6}{r^6} \;+\; \mathfrak{D}_e \;=\; \mathfrak{D}_e\left[\left(\frac{r_e}{r}\right)^6 - \;1\right]^2 \tag{6.32}$$

which supports 24 vibrational levels, the lower panel of Fig. 6.5 shows a plot of that potential and indicates the positions of the energies and turning points of selected levels. The upper panel then shows the nature of the integrand in Eq. (6.31) for those four levels; note that while the integrand goes to infinity at both turning points, the area under the curve is always finite. It is immediately clear that for the higher vibrational levels, the area under the curve – and hence the value of the integral – is increasingly dominated by the nature of the integrand (i.e., of the potential) in the long-range region near the outer turning point.

From the early days of quantum mechanics it has been known that at long range all atomic and molecular interaction potentials become a sum of inverse-power terms

$$V(r) \;\simeq\; \mathfrak{D} \;-\; \sum_{m\geq n} C_m/r^m \;\underset{\{\text{very large } r\}}{\Longrightarrow}\; \mathfrak{D} - C_n/r^n \quad , \tag{6.33}$$

in which the powers m and coefficients C_m are determined by the nature of the interacting atoms. (A brief summary of the rules governing which terms appear in this sum for a given case is presented in the Appendix.). This suggests that for levels whose outer turning points lie at sufficiently large r for the leading (C_n/r^n) term to dominate the interaction, it would be a reasonable approximation to replace $V(r)$ in Eq. (6.31) by the simple function $V(r) \approx \mathfrak{D} - C_n/r^n$ to obtain

$$\frac{dv}{dG_v} \;\approx\; \frac{1}{2\pi}\,\sqrt{\frac{2\mu}{\hbar^2}}\,\int_{r_1(v)}^{r_2(v)} \frac{dr}{[G_v - (\mathfrak{D} - C_n/r^n)]^{1/2}} \quad . \tag{6.34}$$

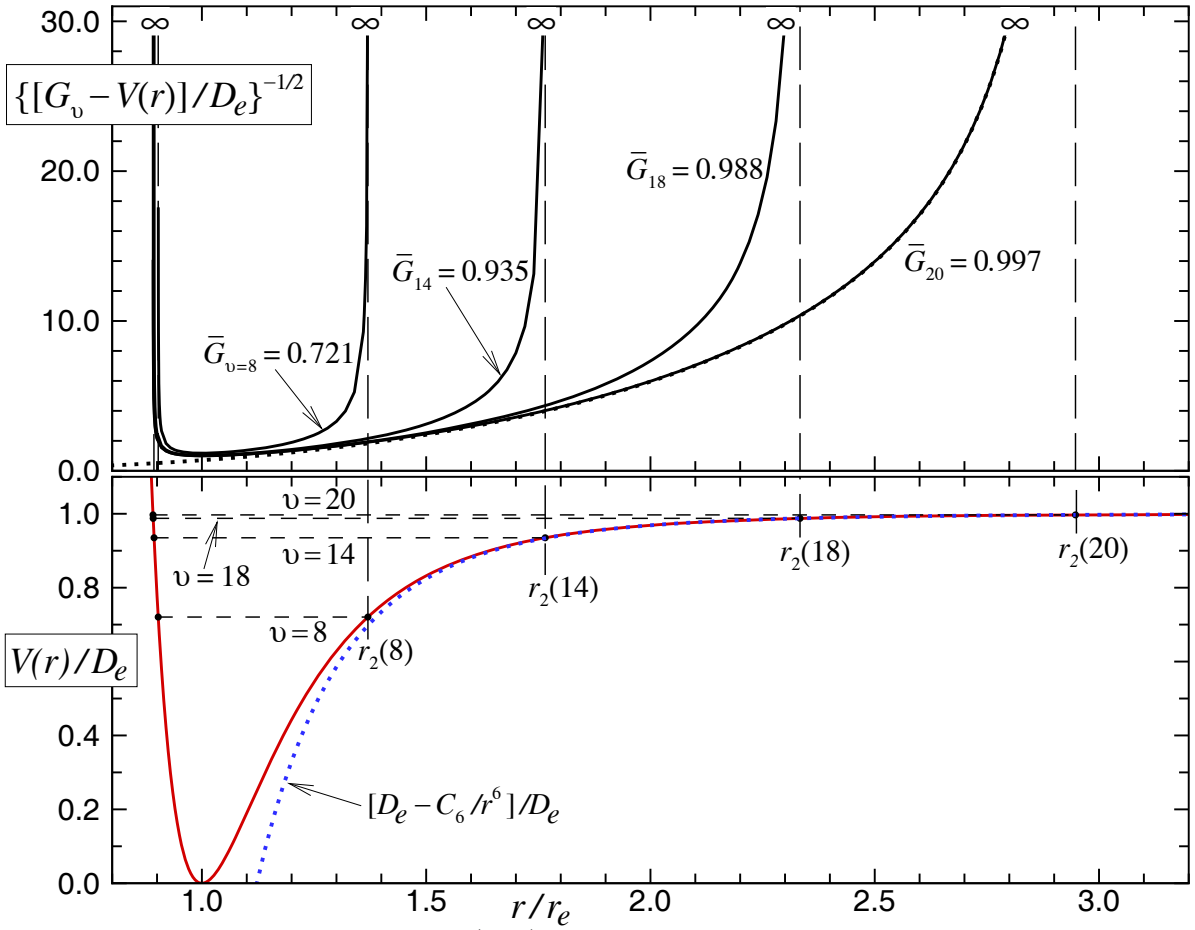

Figure 6.5 Lower Panel: A 23-level LJ(12,6) potential with selected level energies and turning points labelled. Upper Panel: Integrand of Eq. (6.31) for selected levels with $\overline{G}_v \equiv G_v/\mathfrak{D}_e$. (Adapted from Fig. 2 of Ref. [31].)

By making the substitution $y = r/r_2(v)$ and noting that $[G_v - V(r_2(v))] = 0$, and hence that $[\mathfrak{D} - G_v] = C_n/[r_2(v)]^n$, Eq. (6.34) becomes

$$\frac{dv}{dG_v} \approx \frac{1}{2\pi}\sqrt{\frac{2\mu}{\hbar^2}}\frac{(C_n)^{1/n}}{[\mathfrak{D}-G_v\}^{(n+2)/2n}}\int_{r_1/r_2}^{1}\frac{dy}{(y^{-n}-1)^{1/2}} \quad . \tag{6.35}$$

The dotted curve in the Upper Panel of Fig. 6.5 shows what happens to the exact integrand of Eq. (6.31) for level $v = 20$ if the actual potential is replaced by the single inverse-power term $\mathfrak{D} - C_6/r^6$. It is immediately clear that both the effect of this substitution on the value of this integrand and the effect of replacing the lower bound of the integral in Eq. (6.35) by zero will be very small, and will become increasingly negligible for higher vibrational levels (here, $v = 21 - 23$). By making use of the mathematical identity

$$\int_0^1 \frac{dy}{(y^{-n}-1)^{1/2}} = \frac{\sqrt{\pi}}{n}\frac{\Gamma\left(\frac{1}{2}+\frac{1}{n}\right)}{\Gamma\left(1+\frac{1}{n}\right)} \tag{6.36}$$

and inverting the resulting expression, the basic near-dissociation theory (NDT) result is obtained:

$$\frac{dG_v}{dv} = \left\{\frac{2n\sqrt{\pi}}{(C_n)^{1/n}}\sqrt{\frac{\hbar^2}{2\mu}}\frac{\Gamma\left(1+\frac{1}{n}\right)}{\Gamma\left(\frac{1}{2}+\frac{1}{n}\right)}\right\}[\mathfrak{D}-G_v]^{(n+2)/2n} \equiv K_n\,[\mathfrak{D}-G_v]^{(n+2)/2n} \quad . \tag{6.37}$$

It is usually more convenient to work with the integrated form of this equation; this is the central result that

$$G_v = \mathfrak{D} - X_0(n)\left(v_{\mathfrak{D}} - v\right)^{2n/(n-2)} \quad , \tag{6.38}$$

in which $X_0(n) = \left[\frac{(n-2)}{2n}\, K_n\right]^{2n/(n-2)}$. For $n > 2$ the integration constant $v_{\mathfrak{D}}$ is the non-integer effective vibrational index associated with the dissociation limit – the intercept of the correctly extrapolated Birge-Sponer plot for the given system – and its integer part $\overline{v}_{\mathfrak{D}}$ is the index of the highest vibrational level supported by the given potential. For $n = 1$ this expression becomes the Bohr eigenvalue formula for the levels of a Coulomb potential, and $v_{\mathfrak{D}}(n=1) = -(1+\delta)$, where δ is the Rydberg quantum defect. An attractive $n = 2$ long-range potential is not physically possible for a diatomic molecule, but integration of Eq. (6.37) for that case gives essentially the same exponential eigenvalue expression known from quantum mechanics.

In order to express this result in a practical form, it is convenient to take the first derivative of Eq. (6.38) to obtain

$$\frac{dG_v}{dv} \;=\; \left[\left(\tfrac{2n}{n-2}\right) X_0(n)\right] \left(v_{\mathfrak{D}} - v\right)^{(n+2)/(n-2)} \quad . \tag{6.39}$$

Because the vibrational level energies and level spacings are the actual physical observables, the fact that $[dG_{v'}/dv']_{v'=v+1/2} \approx \Delta G_{v+1/2}$ allows Eqs. (6.37–6.39) to be rearranged to yield the expressions

$$\left(\Delta G_{v+1/2}\right)^{2n/(n+2)} \;=\; [K_n]^{2n/(n+2)} \;\left(\mathfrak{D} - G_{v+1/2}\right) \tag{6.40}$$

$$\left(\mathfrak{D} - G_v\right)^{(n-2)/2n} \;=\; [X_0(n)]^{(n-2)/2n} \;\left(v_{\mathfrak{D}} - v\right) \tag{6.41}$$

$$\left(\Delta G_{v+1/2}\right)^{(n-2)/(n+2)} \;=\; \left[\left(\tfrac{2n}{n-2}\right) X_0(n)\right]^{(n-2)/(n+2)} \;\left(v_{\mathfrak{D}} - v - 1/2\right) \quad . \tag{6.42}$$

Near-dissociation theory therefore predicts that if the observable quantities on the left hand side of these equations are plotted *vs.* the vibrational mid-point energy $G_{v+1/2} \approx \frac{1}{2}(G_{v+1} + G_v)$ (for Eq.(6.40)) or the vibrational quantum number v (for the other two equations), for levels lying close to dissociation those plots should be precisely linear, with slopes defined by the constants K_n or $X_0(n)$ (i.e., by μ, n and C_n), while the intercept determines either the energy at the dissociation limit $\mathfrak{D}$ or the vibrational intercept $v_{\mathfrak{D}}$. Plots of this type, sometimes called 'Le Roy–Bernstein plots', are often used to illustrate applications of near-dissociation theory.

Near-dissociation theory expressions analogous to Eq. (6.38) have been reported for a number of other properties, such as expectation values of the kinetic energy or of powers of the internuclear distance, and for values of the rotational constants B_v, D_v, H_v, ... , etc. While it has little direct import for the present discussion, it is interesting to note the algebraic structure of the latter, as it explains the reason for the subscript on the symbol $X_0(n)$ appearing in Eq. (6.38). In particular, for levels lying very near the dissociation limit:

$$B_v \;=\; X_1(n) \left(v_{\mathfrak{D}} - v\right)^{\frac{2n}{n-2}-2} \tag{6.43}$$

$$-\,D_v \;=\; X_2(n) \left(v_{\mathfrak{D}} - v\right)^{\frac{2n}{n-2}-4} \tag{6.44}$$

$$H_v \;=\; X_3(n) \left(v_{\mathfrak{D}} - v\right)^{\frac{2n}{n-2}-6} \tag{6.45}$$

$$L_v \;=\; X_4(n) \left(v_{\mathfrak{D}} - v\right)^{\frac{2n}{n-2}-8} \quad , \tag{6.46}$$

$$\vdots$$

in all of which $X_k(n) = \overline{X}_k(n) \Big/ \left[\mu^n \left(C_n\right)^2\right]^{1/(n-2)}$ and the $\overline{X}_k(n)$ are known numerical factors [32, 31].

One type of application of these results is summarized by Fig. 6.6. It illustrates an NDT treatment of data for the ground electronic state of the very weakly bound Van der Waals molecule Ar_2, which was first observed in 1970 [33]. The square symbols represent the experimental vibrational level spacings and the dash–dot–dot line is the conventional linear Birge-Sponer (B-S) extrapolation (left-hand ordinate axis) reported by the experimentalists, while the shaded area defines their estimate of the distance from the highest observed level ($v = 4$) to the dissociation limit. This approach clearly predicts that $v = 5$ is the highest bound level of this molecule.

As with all molecular states formed from atoms in electronic S states, $n = 6$ for the ground electronic state of Ar_2 (see Appendix). The round symbols in Fig. 6.6 then show exactly those same experimental data

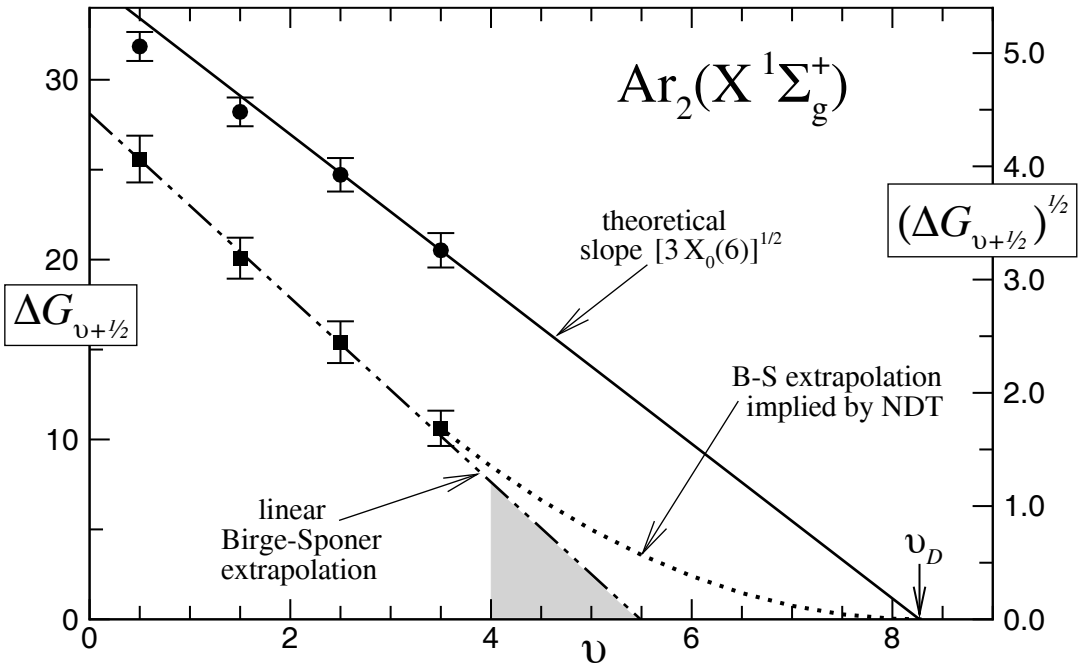

Figure 6.6 Illustrative application of NDT to data for Ar_2. Left Axis: square points, dash-dot-dot line and dotted curve; Right Axis: round points and solid line. (Adapted from Fig. 1 of Ref. [34].)

plotted (against the right-hand axis) in the manner suggested by Eq. (6.42). Since the data for the lowest bound levels are not expected to obey the NDT equation, a simple linear fit to these data could not be trusted to provide a reliable extrapolation. However, an accurate value of the C_6 coefficient for this species was available from *ab initio* quantum mechanical calculations, so the expected limiting slope of this plot could be predicted from the resulting known value of the $X_0(n)$ coefficient. The solid line on this plot shows the NDT prediction of the extrapolation obtained when a line with this theoretical slope passes through the experimental datum for $v = 3$. The fact that the second-last point also lies on this line while those for the two larger level spacings only gradually deviate from it attests to the validity of this extrapolation. The value of $v_{\mathfrak{D}} = 8.27$ implied by this NDT extrapolation shows that this molecule actually has 50% more bound levels than were implied by the linear B-S type extrapolation, and comparison of the shaded area with the area under the dotted curve in the extrapolation region shows that the estimate of the distance from the highest observed level to dissociation yielded by the traditional linear B-S extrapolation was more than a factor of two too small [34].

A second type of application of NDT is the use of Eq. (6.41) in the analysis of 'photoassociation spectroscopy' (PAS) data, for which the measured observable is the binding energy $[\mathfrak{D} - G_v]$. The $1\,^1\Sigma_u^+$ state of Yb_2 dissociates to yield one $^1S_0$ atom and one $^1P_1$ atom, a case for which $n = 3$ (see Appendix). Hence, Eq. (6.41) shows that for levels lying near dissociation, a plot of $[\mathfrak{D} - G_v]^{1/6}$ is expected to be linear with a slope of $[X_0(3)]^{1/6}$ determined by the value of the C_3 coefficient for this state, and the intercept by its $v_{\mathfrak{D}}$ value. Figure 6.7 shows a plot of this type based on the recent results of Takahashi and co-workers [35]. The precise linearity of the points on Fig. 6.7 over a range of almost 80 vibrational levels is a very strong endorsement of the validity of Eqs. (6.38–6.42), and it illustrates the fact that NDT provides the most reliable methods known for experimentally determining values of long-range C_n potential function coefficients.

The two cases considered above both represent situations in which experimental data are available for levels lying sufficiently close to dissociation that NDT may be expected to be valid there. However, for the much more common situations in which this is not true, NDT still offers a valuable means for obtaining optimal estimates of the distance from the highest observed levels to dissociation, and of the number and energies of unobserved levels. In particular, 'near-dissociation expansion' expressions (NDEs), which combine the limiting functional behaviour of Eq. (6.38) with empirical expansions which account for deviations from that limiting behaviour, were introduced to address this problem. Most work with NDEs has involved the

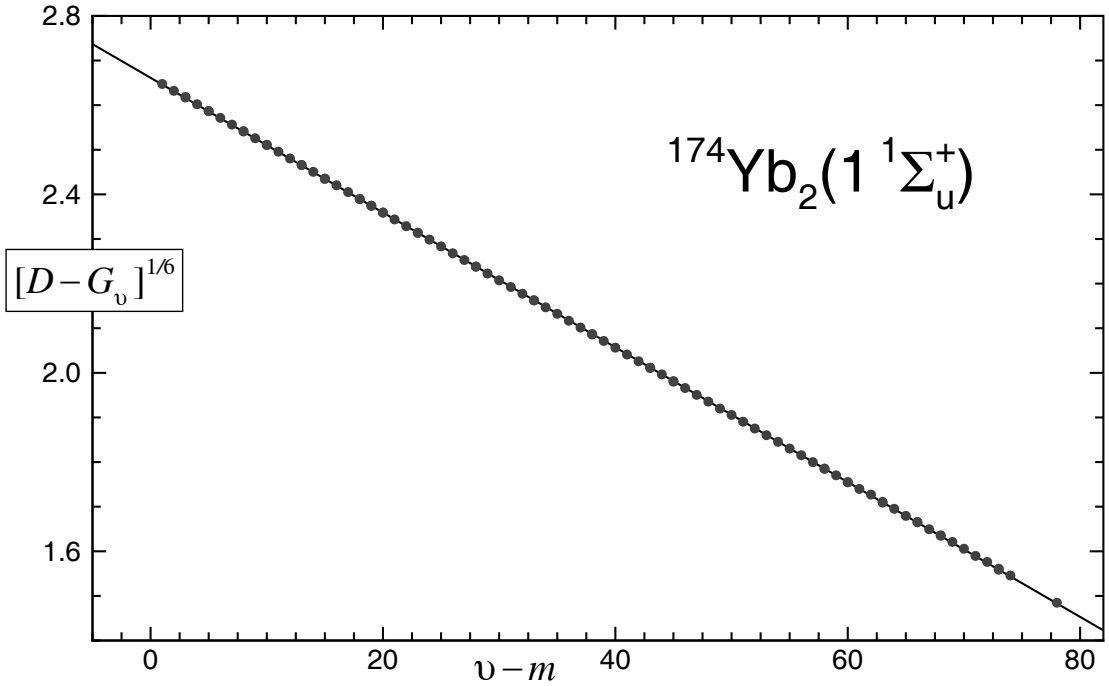

Figure 6.7 Illustrative application of NDT to data for a state of Yb_2 for which $n = 3$. The unspecified integer m indicates that the absolute vibrational assignment is not known.

use of rational polynomials in the variable $(v_{\mathfrak{D}} - v)$:

$$G_v \;=\; \mathfrak{D} \;-\; X_0(n)\,\big(v_{\mathfrak{D}} - v\big)^{2n/(n-2)}\;\big[L/M\big]^s \quad . \tag{6.47}$$

The power 's' in Eq (6.47) is set at either $s = 1$ (to yield 'outer' expansions) or $s = 2n/(n-2)$ (to yield 'inner' expansions), while $[L/M]$ is given by

$$\big[L/M\big] \;=\; \frac{1 \;+\; \sum_{i=1}^{L}\, p_{t+i}\,(v_{\mathfrak{D}} - v)^{t+i}}{1 \;+\; \sum_{j=1}^{M}\, q_{t+j}\,(v_{\mathfrak{D}} - v)^{t+j}} \quad , \tag{6.48}$$

with the value of t being determined by the theoretically known form of the leading correction to the limiting behaviour of Eq. (6.38) [36].

The fundamental *ansatz* underlying the use of NDEs is that fitting experimental data to expressions which incorporate the correct theoretically known limiting near-dissociation behaviour (such as Eq. (6.47)) will yield more realistic estimates of the physically significant extrapolation parameters $\mathfrak{D}$ and $v_{\mathfrak{D}}$ than could otherwise be obtained. In effect, it replaces *blind empirical extrapolation* using Dunham-type polynomials, with *interpolation* between experimental data for levels in the lower part of the potential well and the exactly known functional behaviour near the dissociation limit. Moreover, such expressions often provide more compact representations of the data than do conventional power series in $(v + 1/2)$.

Figure 6.8 summarizes the results of performing NDE fits to experimental data for the $A\,^2\Pi$ state of $MgAr^+$ [37]. Since this species is a molecular ion, the (inverse) power of the leading term in its long-range potential is $n = 4$, and since at least one of its dissociation fragments is in an S state, the power of the second term is $m = 6$ (see Appendix). For this case, theory shows that the power t in Eq. (6.48) should be $t = 2$ [36]. Theory also tells us that for *any* molecular ion, the value of the C_4 coefficient in atomic units is $\alpha/2$, with α being the polarizability of the neutral dissociation fragment, so that the value of the limiting NDT coefficient $X_0(4)$ is readily obtained. Moreover, a good theoretical estimate of the C_6 coefficient could be generated for this state, so a realistic value of the leading-deviation coefficient p_2 (for fixed $q_2 = 0$) could also obtained [37].

The dotted line in Fig. 6.8 shows the limiting slope $[4\,X_0(4)]^{1/3}$ defined by the known C_4 coefficient, while the dot-dash curve labelled "linear B-S extrapolation" shows the extrapolation behaviour implied by a linear

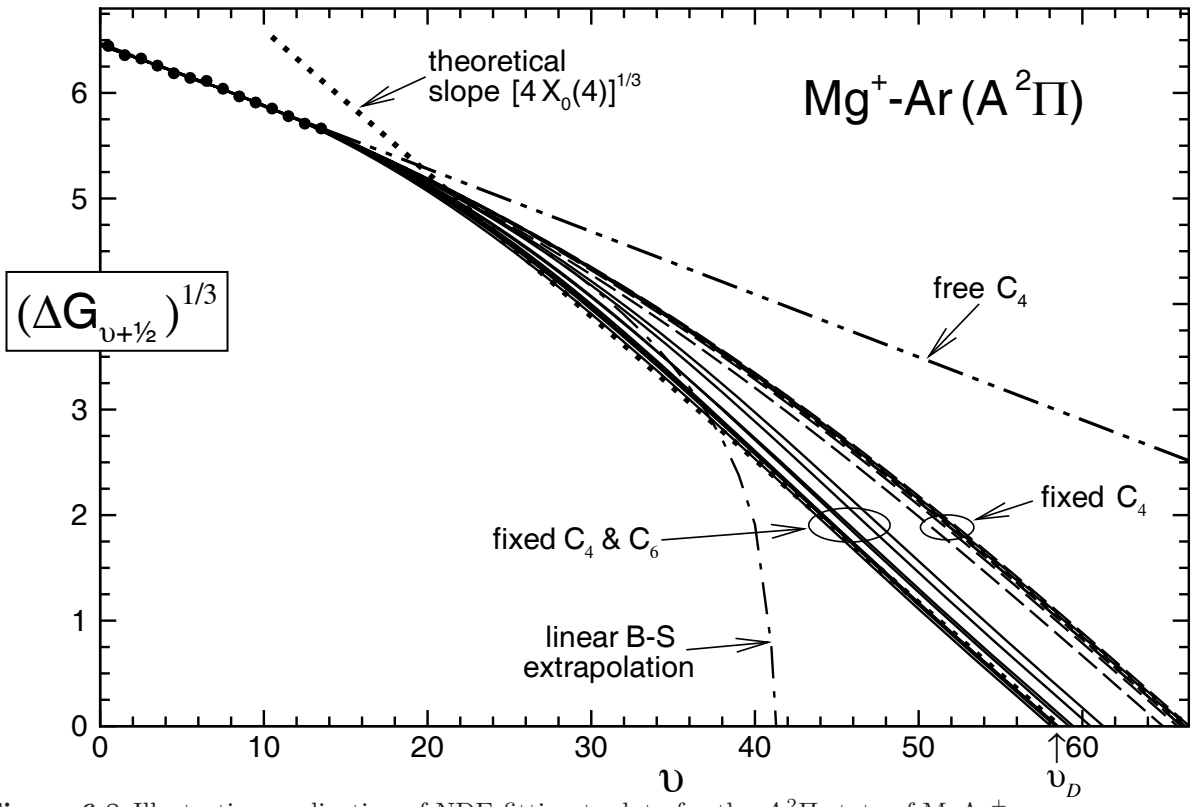

Figure 6.8 Illustrative application of NDE fitting to data for the $A\,^2\Pi$ state of $MgAr^+$.

Birge-Sponer plot. The cluster of seven dashed curves shows the results of NDE fits for different $\{L, M, s\}$ in which the C_4 coefficient was held fixed at the theoretical value and two $\{p_i, q_j\}$ parameters were allowed to vary, with no C_6-based constraint being applied to the p_2 value. The cluster of nine solid curves then shows the results of fits in which both $X_0(C_4)$ and $p_2(C_4, C_6)$ were fixed at the theoretical values, and again two $\{p_i, q_j\}$ parameters were allowed to vary (as well as $v_{\mathfrak{D}}$ and $\mathfrak{D}$). The quality of fit for all of these cases was essentially the same. It is clear that for a given type of model (i.e., only $X_0(4)$ fixed, *vs.* $X_0(4)$ and p_2 fixed), the NDE models corresponding to different choices of $\{L, M, s\}$ are in reasonably good agreement with one another. However, the difference between the extrapolation behaviour for these two classes of models shows that when better theoretical constraints are applied, significantly better extrapolation behaviour is attained. For reference, the dash-dot-dot curve labelled "free C_4" shows that in the absence either of a realistic value of the leading long-range C_n coefficient or of data for levels lying near dissociation, NDE fits can give quite unrealistic extrapolations, and should not be trusted.

A final point raised by the above example is the question of model-dependence, which is an ever-present, but usually ignored problem in scientific data analysis. While all of the nine models corresponding to "fixed C_4 & C_6" give fits to the data of equivalent quality, they all extrapolate slightly differently, and the associated values of the physically interesting parameters $\mathfrak{D}$ and $v_{\mathfrak{D}}$ differ by substantially more than the parameter uncertainty associated with any individual fit. In cases such as this there is no possibility of selecting a unique 'best' model, since there is no physical basis for choosing one set of $\{L, M, s\}$ values over another. The best that one can do is to consider as wide a range of models as possible, and then average the resulting values of the physically interesting parameters and estimate their uncertainties based on both the variance about their mean and the uncertainties in the individual values. A practical scheme for accomplishing this which was introduced in Ref. [37] led to the value of $v_{\mathfrak{D}} = 58.4(\pm 1.2)$ indicated by the pointer at the bottom of Fig. 6.8.

Upon completion of a study such as that illustrated by the results shown in Fig. 6.8, a representative 'optimal' NDE function for the vibrational energies could then be chosen and employed in an RKR calculation to generate a potential spanning essentially the entire potential energy well. Analyses of this type have been

carried out for a number of molecular systems. In general, fits of vibrational energies and rotational constants to NDEs tend to be somewhat more compact that conventional Dunham polynomials – fewer parameters being required to yield a given quality of fit. However, the inter-parameter correlation increases rapidly with the number of free $\{p_i, q_j\}$ parameters, and it becomes increasingly difficult to obtain sufficiently realistic preliminary estimates of those parameters for the non-linear fit to be stable.

Tellinghuisen and Ashmore addressed this fit stability problem by introducing 'mixed representations' for G_v and B_v, in which conventional Dunham polynomials are used at low–v and NDEs at high–v, with a switching function merging the two domains [38, 39]. Such representations certainly work, and they have been implemented in standard data analysis [40] and RKR programs [27]. However, the increased inconvenience associated with these mixed representations makes them somewhat inconvenient to use, and (to date) neither pure NDEs nor these mixed representations have been widely adopted. Indeed, in recent years the whole approach of attempting to provide global descriptions of molecular vibrational-rotational energies using expansions in terms of vibration-rotation quantum numbers is increasingly being supplanted by the 'direct-potential-fit' approach described in § 6.3.

6.2.4 Conclusions Regarding Semiclassical Methods

Since 1932, fits to the Dunham eigenvalue expression of Eq. (6.16) have been a central tool in empirical analyses of diatomic molecule spectroscopic data, and since the mid 1960's, use of the resulting G_v and B_v expressions in the RKR procedure has been a ubiquitous technique for determining diatomic potential energy functions. Replacing Dunham expansions by NDEs or the 'mixed representation' functions described in § 6.2.3 offered a way of addressing a primary weakness of the Dunham polynomial description – namely, its inability to provide realistic extrapolation behaviour. However, the undesirable complication of the latter and the inconvenience of having to perform non-linear least-squares fits which require realistic trial parameters seems to have discouraged widespread use of these two approaches. Moreover, a number of more general shortcomings limit the utility and accuracy of determining potential functions in this way.

(i) The RKR method is a first-order semiclassical procedure that lacks full quantum mechanical accuracy, a problem that is most serious for species of small reduced mass (see Table 6.1).

(ii) It is inconvenient to work with a potential defined by a large array of multi-digit turning points that have to be interpolated over and extrapolated beyond to yield the type of smooth uniform mesh of function values required for use in practical calculations. This step also introduces the spectre of 'interpolation noise' – uncertainties in calculated properties associated with the choice of a particular interpolation scheme – a problem that is usually simply ignored.

(iii) The RKR method of § 6.2.2 is based on the fact that determination of the potential function requires only a knowledge of G_v and B_v. However, the discussion of § 6.1 pointed out that exact quantum mechanical values of diatomic molecule centrifugal distortion constants (CDCs) $\{D_v, H_v, L_v. \ \ldots\}$ (the derivatives of the energy with respect to $[J(J+1)]$ evaluated at $J=0$) can be calculated from any given potential energy function. Thus, CDCs are not independent parameters, but are implicitly determined by the G_v and B_v functions. In spite of this, in most published data analyses the centrifugal distortion expansion coefficients (i.e., the Dunham $Y_{\ell,m}$ coefficients with $m \geq 2$) have been treated as independent free parameters. As a result, errors in the fitted CDCs would introduce small compensatory errors into the B_v functions used to define the potential. Over the last 25 years it has become increasingly common to address this problem by performing self-consistent data analyses in which CDC constants calculated from a preliminary RKR potential are held fixed in a new fit to the global data set to obtain improved G_v and B_v functions, and hence a better RKR potential. Iteration of this procedure generally converges quickly. However, its use does complicate empirical data analyses.

(iv) Combined-isotopologue data analysis fits can be performed using versions of Eq. (6.16) which include atomic-mass-dependent terms to account both for Born-Oppenheimer breakdown effects and for the breakdown of the simple reduced-mass scaling implied by the first-order semiclassical quantization condition [40]. However, there is no simple way for distinguishing between these two types of corrections; as a result, Born-Oppenheimer breakdown contributions to the interaction potential cannot be readily determined in this way.

In view of these concerns, there is clearly a need for the type of exact quantum mechanical data analysis procedure for determining global analytic potential energy functions described in § 6.3. Nonetheless, the semiclassical methods described in § 6.2 remain valuable for several reasons. One of these is simply the fact that they are friendly, familiar, and fairly easy to apply. A more fundamental reason, however, is the fact that the methods of § 6.3 always involve non-linear least-squares fits that require realistic initial trial parameters if the fit is to be at all stable (see Chapter 2), and this traditional methodology provides an excellent way of generating such trial parameters (see § 6.3.3). Moreover, use of NDT remains the best way known for extrapolating beyond observed vibrational data to determine bond dissociation energies, as well as for determining experimental values of the leading long-range inverse-power C_n coefficient. As a result, it remains a central tool in the interpretation and analysis of PAS measurements and other types of data for levels lying very near dissociation. Thus, it can be anticipated that the semiclassical methods described above will remain essential tools in a spectroscopist's arsenal for the foreseeable future.

6.3 Quantum-Mechanical Direct-Potential-Fit Methods

6.3.1 Overview and Background

In recent years it has become increasingly common to analyze diatomic molecule spectroscopic data by performing 'direct potential fits' (DPFs), in which observed transition energies are compared with eigenvalue differences calculated from an effective radial Schrödinger equation based on some parameterized analytic potential energy function, and a least-squares fit is used to optimize the parameters defining that potential. The effective radial Hamiltonian may also include radial strength functions that characterize atomic-mass-dependent adiabatic and non-adiabatic Born-Oppenheimer breakdown (BOB) functions, and also (if appropriate) radial strength functions that account for splittings due to angular momentum coupling in electronic states with non-zero electronic angular momentum. As the well depth and equilibrium bond length are usually central parameters of the potential function model, these equilibrium properties are determined directly from the fit. The DPF approach was originally introduced for the treatment of atom-diatom Van der Waals molecules, for which the lack of any well-defined structure precluded the effective use of traditional methods of analysis [41]. However, over the past two decades it has become increasingly widely used for diatomic data analyses.

The essence of the method is as follows. The upper and lower levels of any observed spectroscopic transition are eigenvalues of Eq. (6.1) for the appropriate effective potential energy function. As discussed in § 6.1, for any given potential this equation can be solved readily using standard methods to yield the eigenvalue $E_{v,J}$ and eigenfunction $\psi_{v,J}(r)$ of any given vibration-rotation level $\{v, J\}$. Moreover, the Hellmann-Feynman theorem shows that the partial derivative of that eigenvalue with respect to any given potential function parameter p_j may be calculated using the expression

$$\frac{\partial E_{v,J}}{\partial p_j} \;=\; \left\langle \psi_{v,J}(r) \left| \frac{\partial V(r)}{\partial p_j} \right| \psi_{v,J}(r) \right\rangle \quad . \tag{6.49}$$

The difference between such derivatives for the upper and lower level of each observed transition is the partial derivative of that datum with respect to parameter p_j required by the least-squares fitting procedure.

One challenge of this approach is the fact that the data set often consists of many thousands or tens of thousands of individual transitions involving a wide range of vibration-rotation levels, which means that being able to solve Eq. (6.1) efficiently is a matter of some importance. It is always necessary for the Schrödinger-solver subroutine to start from a realistic initial trial energy for each level of interest, and the more accurate the initial estimate, the smaller the time required for obtaining the desired solution. One way of addressing this challenge is as follows. Prior to beginning the fit, the data set would be surveyed to determine the highest observed vibrational level for each electronic state considered. Then at the beginning of each cycle of the non-linear fit to optimize the potential function parameters, an automatic procedure would locate each of those (pure) vibrational levels. A particularly efficient way of doing this would make use of semiclassical energy derivatives computed using Eq. (6.31) to generate an estimate of the distance from a given level to the next. Once the pure vibrational levels are known, Hutson's method (Refs. [6] & [7] see § 6.1) may be used to generate values of the first few rotational constants for each vibrational level. As the

fitting procedure considers the data one at a time, these stored band constants can be used in Eq. (6.4) to generate a good initial estimate of the required initial trial energy for the level in question. This combined quantum/semiclassical procedure is quite efficient.

Two other key problems associated with DPF treatment of diatomic molecule data are what potential function form to use, and how to obtain the realistic initial trial parameters required by the non-linear least-squares fitting procedure. These topics are discussed in the next two subsections.

6.3.2 Potential Function Forms

A central challenge of the DPF method has been the problem of developing an optimum analytic potential function form. Ideally, such a function should satisfy the following criteria.

- It should be flexible enough to represent very extensive, high-resolution data sets to the full degree of experimental accuracy.
- It should be robust and well-behaved, with no spurious extrapolation behaviour outside the region to which the experimental data are most sensitive.
- It should be smooth and continuous everywhere.
- It should incorporate the correct theoretically known limiting behaviour of Eq. (6.33) at large distances.
- It should be compact and portable – i.e., be defined by a relatively modest number of parameters.

Devising a potential function form that satisfies all of these criteria has been a non-trivial problem, and work on developing new and better forms ('potentiology') remains an active area of research. The following subsections describe and compare four families of potential function forms that have been used in diatomic DPF analyses.

A. Polynomial Potential Function Forms

The oldest type of potential function form used in DPF data analyses consists of a simple polynomial expansion in a radial-coordinate such as the Dunham variable $\xi_{\rm Dun}=(r-r_e)/r_e$ (see Eq. (6.14)). Dunham expansions themselves have the obvious shortcoming that $V_{\rm Dun}(r) \rightarrow +\infty$ or $-\infty$ as $r \rightarrow \infty$, the sign depending on the sign of the last non-zero polynomial coefficient. However, this singularity problem is resolved if the Dunham radial variable is replaced by an alternative such as that proposed by Ogilvie and Tipping [42]

$$\xi_{\rm OT}(r) \;=\; 2\left(\frac{r-r_e}{r+r_e}\right) \quad . \tag{6.50}$$

This variable has the nice property that it approaches finite values at the two limits $r \rightarrow 0$ and $r \rightarrow \infty$, so a potential energy function defined as a power series in this variable will have no singularities. Moreover, the simplicity of such power-series forms makes it very easy to generate expressions for the partial derivatives of the potential function required for calculating partial derivatives of the observables using Eq. (6.49). However, the resulting potentials may still behave unphysically outside the range of the data employed for their determination.

We recall from the discussion of § 6.2.3 that at long range all intermolecular potentials take on the the inverse-power-sum form of Eq. (6.33). In principle, polynomial functions of $\xi_{\rm OT}(r)$ may be constrained to approach a specified asymptote in this way [43]. However, the expressions required to impose this behaviour are quite complex and require the inclusion of multiple additional polynomial coefficients. For example, requiring a potential function defined as a polynomial in the coordinate $\xi_{\rm OT}$ to approach an asymptote with a specified $V(r) \sim \mathfrak{D} - C_6/r^6$ limiting behavior would require that polynomial to have *seven* additional high-order terms beyond those required to represent the experimental data. While this is mathematically straightforward, the resulting functions have an unfortunate tendency to be somewhat unstable and to display spurious oscillatory behaviour in the interval between the data region and the limiting long-range region. Thus, a simple polynomial in a variables such as $\xi_{\rm OT}$ is not a viable way of describing an overall potential energy function.

The problem of imposing a constraint on the long-range behaviour of a polynomial potential function is somewhat reduced if one uses a radial variable of the type proposed by Šurkus [44]:

$$\xi^{(p)}_{\check{\rm Sur}}(r) \;=\; \frac{r^p - (r_e)^p}{r^p + (r_e)^p} \;\equiv\; y^{\rm eq}_p(r) \tag{6.51}$$

At large distances $\xi^{(p)}_{\check{\rm Sur}} \simeq 1 - 2(r_e/r)^p + \ldots$, so if p is set equal to the power (n) of the leading inverse-power term in the long-range potential, it is a fairly straightforward matter to constrain such a potential function to have the desired limiting $\mathfrak{D} - C_n/r^n$ behaviour. However, when the power p has a moderately large value, such as $p = 6$, $\xi^{(p)}_{\check{\rm Sur}}(r)$ is relatively 'stiff' (see § 6.3.2 B), and hence a polynomial based on it will have limited flexibility. Moreover, it would be impossible to constrain such a polynomial to mimic more sophisticated long-range behaviour, such as $V(r) \simeq \mathfrak{D} - C_6/r^6 - C_8/r^8$. Hence, potential energy functions defined as polynomials in a Šurkus variable with large p are of limited use.

A practical way to circumvent the problem of the poor long-range behaviour of polynomial potential functions is simply to attach the desired long-range inverse-power-sum tail smoothly to the fitted polynomial at some point near the outer end of the data-sensitive range of r. This has been the approach used by a group at the University of Hannover in a large number of very careful studies of alkali metal and alkaline earth diatomics, for many of which the data span almost the entire potential energy well. They represent the potential energy function within the 'data range' by a polynomial in the variable $\xi_{\rm Han} = (r - r_m)/(r + b\, r_m)$ in which r_m is a fixed distance located near r_e, and 'b' is a fitted constant [45]. However, *no* polynomial is reliable outside the range of the data to which is it fitted, so to obtain a useful overall potential function it is always necessary to attach both some simple repulsive analytic function at the inner end of the data region and the desired inverse-power-sum at the outer end. Although these extrapolation functions are parameterized so that they attach to the polynomial smoothly, the point of attachment remains an *ad hoc* choice. Moreover, the whole attachment procedure relies on the fact that the polynomial potential energy *and* its first derivative are both physically correct at the extreme ends of the data-sensitive region, a sometimes questionable assumption. This type of potential form also has three other worrisome shortcomings.

(1) The polynomials required to account fully for the data often have very high orders – orders between 20 and 40 being common for extensive experimental data sets. Fits to polynomials of such high order tend to be very highly correlated, and sometimes convergence is difficult to achieve.

(2) While the independent variable typically spans the range $\xi_{\rm Han} \in (-0.1,\, 0.6)$ and the potential function on that domain spans an energy range of order 10^4 cm^{-1}, the higher-order polynomial coefficients are usually of oscillating sign and have magnitudes as much as $4 - 8$ orders of magnitude greater than the range of the function being fitted. This is a signature for a marginally stable model.

(3) In most published analyses using this form, all of the (many) potential coefficients reported are listed to 18 significant digits. This means that quadruple-precision arithmetic would be needed to reproduce these functions on most computers, a point that can make such potentials somewhat inconvenient for others to use. Moreover, if the parameters of any model describing data (such as energy level spacing) known to $6 - 8$ significant digits truly requires its parameters to be specified to 18 significant digits, there must be something wrong with the model.

In summary, although a number of very extensive, high-resolution data sets have been fitted accurately using polynomial potentials, such functions do not represent an optimum way of summarizing what is known about a molecule.

B. The 'Expanded Morse Oscillator' (EMO) Potential Form, and the Importance of the Definition of the Expansion Variable

An important development in potential function modeling was the demonstration by Coxon and Hajigeorgiou that a Morse potential with a distance-dependent exponent coefficient was a compact and flexible function that could provide a very accurate representation of a potential energy well [46, 47, 48]. A potential well typically spans an energy range of $10^3 - 10^5$ cm^{-1} and needs to be known to an accuracy of $\lesssim 10^{-3}$ cm^{-1} if it is to explain high resolution experimental data. Coxon and Hajigeorgiou had the insight to realize that the $\mathfrak{D}_e$ value and the algebraic structure of the Morse function would account for the bulk of that change, while

modest variations of the exponent coefficient would allow precise changes in the potential function shape to be defined by a relatively modest number of parameters. In their early work, the Morse function exponent coefficient was represented by a simple power series in r. However, that proved to be inappropriate, since it meant that as $r \to \infty$ the exponent coefficient polynomial would approach either $+\infty$ or $-\infty$ (depending on the mathematical sign of the highest-order expansion coefficient). Such singularities are removed if the power series expansion variable is replaced by a quantity such as $\xi_{\rm OT}(r)$ (see Eq. (6.50)), but problems remain, since the value of the expansion variable at the outer end of the data region remains a long way from its limiting value [49]. However, a more robust model is obtained if a version of the Šurkus variable of Eq. (6.51) with $p \gtrsim 3$ is used as the exponent expansion variable [50, 51, 52].

The resulting model is called the 'Expanded Morse Oscillator' (EMO) potential:

$$V_{\rm EMO}(r) \;=\; \mathfrak{D}_e \left(1 \;-\; e^{-\beta(r)\cdot(r-r_e)}\right)^2 \quad , \tag{6.52}$$

in which

$$\beta(r) \;=\; \beta_{\rm EMO}(r) \;=\; \sum_{i=0}^{N} \beta_i \, \left(y_p^{\rm ref}(r)\right)^i \quad , \tag{6.53}$$

with

$$y_p^{\rm ref}(r) \;=\; y_p(r;r_{\rm ref}) \;=\; \frac{r^p - (r_{\rm ref})^p}{r^p + (r_{\rm ref})^p} \quad . \tag{6.54}$$

In all currently published work using this model, the reference distance in the expansion variable was set as $r_{\rm ref} \equiv r_e$. However, recent work using the related 'MLR' model (described below) shows that fixing the exponent-expansion-variable reference distance $r_{\rm ref}$ at a value larger than r_e, typically in the range $1.2\,r_e - 1.5\,r_e$, allows accurate fitted potential functions to be obtained that require a substantially smaller number of β_i expansion coefficients than would otherwise be needed [53, 54].

One other key feature of this model is the power 'p' in the definition of the radial expansion variable. For $p = 1$, the values of $y_p^{\rm ref}(r)$ at the inner and outer ends of the data region are a long way from their limiting values of -1 and $+1$, respectively. As a result, a moderately high-order polynomial function of that variable will have a high probability of behaving poorly (e.g., showing oscillatory behaviour) on the intervals between the data region and the $y_p = \pm 1$ limits. As p increases, however, the mapping of $y_p(r)$ onto r places the values of $y_p(r)$ at the inner and outer ends of the data region ever closer to the limiting values of ± 1, and hence removes the possibility of such misbehaviour.

The importance of being able to set $p > 1$ and $r_{\rm ref} > r_e$ is illustrated by Fig. 6.9, which shows how $y_p(r;r_{\rm ref})$ depends on p and r for the two cases $r_{\rm ref} = r_e$ (solid curves) and $r_{\rm ref} = 1.5\,r_e$ (dashed curves). The vertical broken lines on this plot are the inner and outer ends of the data-sensitive region[2] for the ground $X\,^1\Sigma_g^+$ state of Rb_2, as considered in the analysis of Ref. [54]. For $p = 1$ the variable $y_1(r;r_e)$ at the outer end of the data region is barely half way to its limiting value of $+1$, while $y_1(r;r_{\rm ref} = 1.5\,r_e) \approx 0.33$. Thus, any function of those variables whose coefficients are defined by its behaviour within the data region would have ample opportunity to behave unphysically between the end of the data region and the limit $r \to \infty$. In contrast, for higher values of p the variable $y_p(r)$ at the outer end of the data region becomes relatively flat and close to its upper bound, so that an exponent coefficient function $\beta(r)$ defined as a polynomial in that variable would change very little at larger distances. This bodes well for stable extrapolation behaviour of the associated potential energy function.

The solid curves in Fig. 6.9 show that the fact that $y_p(r;r_e)$ is close to its upper limit at the outer end of the data region does not necessarily mean that the same is true at the inner end; hence (for example), setting $p \gtrsim 3$ does not suffice to ensure sensible inward extrapolation. However, the dashed curves in Fig. 6.9 show that choosing a value of $r_{\rm ref}$ somewhat larger than r_e makes the range of $y_p^{\rm ref}$ more 'symmetric' at the two ends of the data range. Indeed, if $r_{\rm ref}$ is set at the geometric mean of the inner and outer bounds, $r_{\rm ref} = \sqrt{r_{\rm inner} \times r_{\rm outer}}$, the range of $y_p(r;r_{\rm ref})$ will be precisely symmetric on that domain; i.e., $y_p(r_{\rm inner};r_{\rm ref}) = -y_p(r_{\rm outer};r_{\rm ref})$, independent of the choice of p. When combined with an appropriate

[2] Defined here as the inner and outer classical turning points of the highest vibrational level involved in the experimental data set.

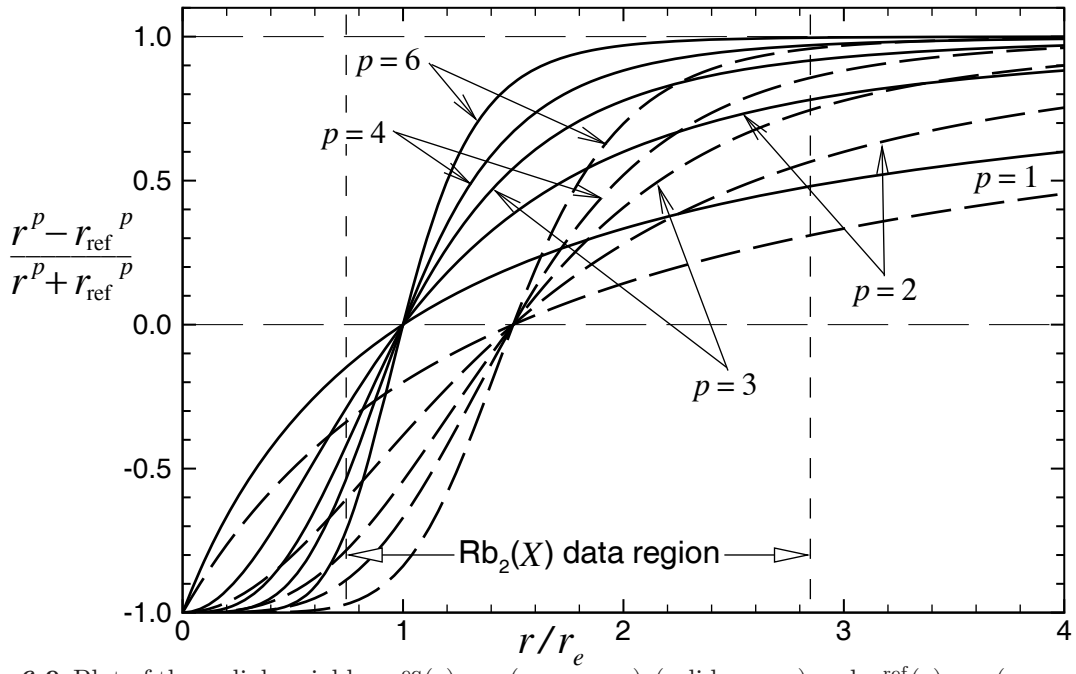

Figure 6.9 Plot of the radial variables $y_p^{\rm eq}(r) = y_p(r; r_{\rm ref} = r_e)$ (solid curves) and $y_p^{\rm ref}(r) = y_p(r; r_{\rm ref} = 1.5\, r_e)$ (dashed curves) for various p, and the data-sensitive region for ground-state Rb_2.

choice of $p > 1$, setting $r_{\rm ref}$ at an appropriate value greater than r_e will ensure stable extrapolation past both the inner and the outer ends of the data region.

The EMO potential form has been used in a number of empirical data analyses, yielding accurate analytic potential functions that fully reproduce the experimental data considered, giving very good estimates of the equilibrium distance r_e, and (if $\mathfrak{D}_e$ is a fitting parameter) also giving a realistic estimate of the well depth. Indeed, this potential function form satisfies all of the criteria itemized in § 6.3.1 except one: its fundamental exponential-type nature means that it cannot incorporate the inverse-power-sum behaviour characteristic of all long-range interatomic potentials. For molecular states with simple single-well potentials for which no realistic estimates of the leading long-range inverse-power C_m coefficients are known, the EMO form is arguably the best model potential function available. However, if values of the C_m coefficients are known, it is always better to incorporate the theoretically predicted inverse-power behaviour into the potential using the type of model potential energy function described in the following subsection.

C. The Morse/Long-Range (MLR) Potential Form

The potential function form described in this section has the same basic algebraic structure as the Morse-type potential of § 6.3.2 B, but it incorporates two key differences. The first is the replacement of the exponent distance factor $(r - r_e)$ in Eq. (6.52) by the variable $y_p^{\rm eq}(r)$ of Eq. (6.51); the second is the introduction of a pre-exponential factor to incorporate the desired long-range behaviour. The resulting function is

$$V_{\rm MLR}(r) \;=\; \mathfrak{D}_e \left(1 \;-\; \frac{u_{\rm LR}(r)}{u_{\rm LR}(r_e)} \; e^{-\beta(r) \cdot y_p^{\rm eq}(r)} \right)^2 \quad . \tag{6.55}$$

The fact that $y_p^{\rm eq}(r_e) = 0$ and the pre-exponential factor equals unity at $r = r_e$ ensures that this function retains the Morse-type property of having its minimum at r_e and a well depth of $\mathfrak{D}_e$. Since the coefficient function $\beta(r)$ is written as a (constrained) polynomial in $y_p^{\rm ref}(r)$, the exponent in Eq. (6.55) will approach a finite value as $r \to \infty$. If this limiting value of the exponent is defined as

$$\beta_\infty \;\equiv\; \lim_{r \to \infty} \left\{ \beta(r) \cdot y_p^{\rm eq}(r) \right\} \;=\; \lim_{r \to \infty} \left\{ \beta(r) \right\} \;=\; \ln \left(\frac{2\, \mathfrak{D}_e}{u_{\rm LR}(r_e)} \right) \quad , \tag{6.56}$$

then the limiting long-range behaviour of the MLR function will be simply

$$V_{\rm MLR}(r) \;\simeq\; \mathfrak{D}_e \;-\; u_{\rm LR}(r) \;+\; \mathcal{O} \left(\frac{u_{\rm LR}^2}{4\, \mathfrak{D}_e} \right) \quad . \tag{6.57}$$

Thus, if $u_{\rm LR}(r)$ is defined as the sum of inverse-power terms appropriate for the molecular state in question

$$u_{\rm LR} \;=\; \frac{C_{m_1}}{r^{m_1}} \;+\; \frac{C_{m_2}}{r^{m_2}} \;+\; \ldots \;, \tag{6.58}$$

then the long-range tail of the MLR function will have the correct theoretically predicted inverse-power long-range form.

A simple way to constrain the polynomial expression for $\beta(r)$ to approach the limiting value β_∞ as $r \to \infty$ is to write it in the form

$$\beta(r) \;=\; \beta_{\rm MLR}(r) \;=\; y_p^{\rm ref}(r)\;\beta_\infty \;+\; [1 - y_p^{\rm ref}(r)]\;\sum_{i=0}\beta_i\;\left[y_q^{\rm ref}(r)\right]^i \quad . \tag{6.59}$$

However, in order to prevent the leading contributions to the asymptotic expansion of the exponential term in Eq. (6.55) from modifying the long-range behaviour specified by Eq. (6.58), the power p in Eqs. (6.55) and (6.59) must satisfy the condition $p > m_{\rm last} - m_{\rm first}$, where $m_{\rm first}$ and $m_{\rm last}$ are, respectively, the powers of the first and last terms included in the chosen definition of $u_{\rm LR}(r)$ [55]. For states formed from ground-state atoms, the leading terms contributing to the long-range potential energy often correspond to $m = 6$, 8 and 10; if these three terms define $u_{\rm LR}(r)$, it becomes necessary to set $p \geq 5$. Note, however, that there are no restrictions on the value of q, and giving it a somewhat smaller value than p often yields good fits with polynomials of lower-order than would otherwise be required [53, 54].

The basic form of the MLR potential function seen in Eq. (6.55) is remarkably simple, and the fact that the leading terms in the long-range potential energy are explicitly incorporated within its algebraic form rather than being represented *via* a separate attached function is a great improvement over other models. The fact that the empirical function that determines the details of the potential function shape appears in an exponent, together with the use of an expansion variable $y_p^{\rm ref}(r)$ centred at a distance $r_{\rm ref} > r_e$, also make this form particularly flexible, and allow accurate fits to be obtained with a relatively modest number of expansion parameters. Moreover, the physically interesting quantities r_e , $\mathfrak{D}_e$, and C_n are explicit parameters of the MLR model that may be varied in the fit, while for other functional forms the determination of $\mathfrak{D}_e$ and C_m parameters depends partly on where and how the long-range tail is attached to the polynomial spanning the data region.

Illustrations of the importance of the parametrization details described above are provided by the results of DPF analyses of extensive high-resolution data sets for the ground electronic states of MgH and Ca_2 summarized in Table 6.2. In a recently published data analysis for MgH using a simple version of the MLR form which fixed $r_{\rm ref} = r_e$ and $p = q = 4$, an exponent polynomial of order 18 was required to give a good fit, and the resulting higher-order β_i expansion coefficients had alternating mathematical signs and magnitudes of order $10^6 - 10^7$ [56]. The fact that polynomial coefficients of this magnitude are required to represent a function with the range $-2.8 \lesssim \beta(r) \lesssim -0.5$ on the data-sensitive domain $-0.3 \lesssim y_p^{\rm eq}(r) \lesssim 0.6$ is a clear signature of a marginally stable model. In contrast, use of the extended MLR model described above with $r_{\rm ref} = 2.3\,\text{Å} \approx 1.33\,r_e$ and $\{p, q\} = \{5, 4\}$ yields the same quality of fit with an exponent polynomial order of only 14, and the magnitudes of the resulting β_i coefficients ranged from ~ 0.05 to 20, values much more consonant with the domain and range of the function being fitted.

The second case considered in Table 6.2 again shows that employing a more sophisticated MLR form for which $r_{\rm ref} > r_e$ and $q < p$ allows the data to be fully explained by a much more compact function

Table 6.2 Results of fits performed using different potential function models; $\overline{dd}$ is the relative (normalized by the data uncertainties) root-mean-square difference between simulated and experimental transition energies.

			No. parameters			
species	model	$u_{\rm LR}(r)$	polynomial	fitted	total	$\overline{dd}$
$MgH(X\,^1\Sigma^+)$	'basic' MLR	C_6, C_8	19	21	24	0.78
	full MLR	C_6, C_8, C_{10}	15	18	22	0.78
$Ca_2(X\,^1\Sigma_g^+)$	Hannover polynomial	C_6, C_8, C_{10}	21	25	31	0.69
	'basic' MLR	C_6, C_8	12	15	17	0.622
	full MLR	C_6, C_8, C_{10}	8	12	16	0.619

Table 6.3 Comparison of potentials obtained from fits to data for $Ca_2(X\,^1\Sigma_g^+)$ using MLR functions without [55] *vs.* with $r_{\rm ref} > R_e$ and $q < p$. In the model of Ref. [55] the exponent polynomial order was truncated to 4 for $r < r_e$. As in Table 6.2, $\overline{dd}$ is the dimensionless root mean square deviation for the fit to the 3553 data.

	From Ref. [55]	generalized MLR
$\mathfrak{D}_e$ / cm^{-1}	1102.076 ($\pm$0.004)	1102.080 ($\pm$0.004)
r_e / Å	4.27781 ($\pm 0.00002_5$)	4.27782 ($\pm$0.00002)
C_6 /cm^{-1} Å^6	1.032 ($\pm$0.001)$\times 10^7$	1.046 ($\pm$0.003)$\times 10^7$
C_8 /cm^{-1} Å^8	3.096×10^8	3.0608×10^8
C_{10} /cm^{-1} Å^{10}	—	8.344×10^9
$\{p, q\}$	$\{5, 5\}$	$\{5, 3\}$
$r_{\rm ref}$ / Å	$[r_e]$	[5.55]
β_0	−1.074136	−1.46725
β_1	0.0232	−0.20011
β_2	−0.42734	−0.72636
β_3	−0.1602	0.1227
β_4	−0.3443	−0.2763
β_5	−8.228	0.507
β_6	72.177	0.357
β_7	−291.79	1.02
β_8	639.5	—
β_9	−797.5	—
β_{10}	533.	—
β_{11}	−150.	—
$\overline{dd}$	0.622	0.619

than had been obtained using a 'basic' MLR form in which $r_{\rm ref} = r_e$ and $q = p$ [55, 54]. The first Ca_2 entry in this table also shows that a fit to the same data set using a 'Hannover polynomial potential' of the type described in § 6.3.2 A requires many more parameters than either MLR model. Further details for this case are presented in Table 6.3, which compares the parameter sets required to account for the data using the 'basic' (from Ref. [55]) and 'generalized' MLR forms. It is clear that the type of generalized MLR function described above yields a more compact and robust model than do either the 'basic' MLR form or the polynomial potentials of § 6.3.2 A. As a result, fits using this form can be expected to yield more reliable fitted values of physically significant parameters such as $\mathfrak{D}_e$, the equilibrium bond length r_e, and any fitted C_m coefficients.

An instructional observation provided by Table 6.3 concerns parameter uncertainties. The uncertainties in $\mathfrak{D}_e$, r_e and C_6 seen there are the full correlated 95% confidence limit uncertainties in those parameters yielded by the fit to the given model. However, the difference between the C_6 values yielded by these fits of equivalent quality to the same data set is an order of magnitude larger than the parameter uncertainties from the individual fits. This illustrates the fact that that model-dependence – the dependence of a fitted parameter value on the model used for the analysis – is often a much larger source of real uncertainty that is the conventional parameter uncertainty implied by the statistics of a given fit. The only way to estimate the magnitude of uncertainty due to model-dependence is to compare the results of fits performed using a wide variety of models. For the case of Ca_2, this led to estimated uncertainties in $\mathfrak{D}_e$ and r_e of 0.008 cm^{-1} and 0.00003 Å, respectively, only slightly larger that the uncertainties shown in Table 6.3, but for C_6 the analogous estimated total uncertainty of 0.02×10^7 cm^{-1} Å^6 was an order of magnitude larger that the uncertainty implied by the individual fits [55].

The MLR potential function form described in this section is being employed in an increasing number of practical data analyses, and is arguably the best model for a single-well potential energy function developed to date. However, it has not been shown that the exponent-polynomial version of this function described above are able to describe double-minimum or shelf-state potentials accurately. Fortunately, a completely

different type of potential function model has been developed which seems ideally suited for dealing with such cases.

D. The Spline-Pointwise Potential (SPP) Form

A 'Spline-Pointwise Potential' (SPP) is an analytic potential energy function defined as a cubic spline function passing through a chosen grid of points, with the energies of the spline points being the parameters varied in the DPF procedure. This novel approach was first introduced in the late 1980's by Tiemann and Wolf, who applied it to the analysis of their data for a number of systems including species with shallow wells and quasibound levels supported by potential energy barriers arising from potential curve avoided crossings [57, 58, 59, 60]. While remarkable for its time, fits using the original version of this approach tended to be somewhat unstable, and required very careful monitoring. As a result, it saw little further use until the turn of the century when Pashov and co-workers re-discovered it and showed that use of singular-value-decomposition at the core of the least-squares procedure allowed fits using this potential function form to be stable and 'routine' [61, 62, 63].

A cubic spline function is normally thought of as a set of cubic polynomials with a distinct cubic spanning the interval between each pair of adjacent points, while the coefficients are constrained to impose continuity and smoothness at each internal grid point. For DPF applications, however, Pashov and co-workers showed that it was more convenient to write such a spline function as a linear combination of basis functions associated with the N specified mesh points $\{r_i\}$,

$$V_{\rm SPP}(r) \;=\; \sum_{i=1}^{N} \; V(r_i) \; S_i^N(r) \quad , \tag{6.60}$$

in which the potential function values $V(r_i)$ at the grid points r_i are the parameters to be varied in the fits. They also chose to use 'natural' cubic splines, so defined by the fact that the second derivative of the function vanishes at the first and last grid points. This is a very simple function to use, since the partial derivative functions required by the least-squares procedure are the parameter-independent functions $S_i^N(r)$.

SPP functions have been used in successful DPF data analyses for regular single-well potentials, for double-well potentials, and for states whose potential functions have a single well with a rotationless barrier protruding above the asymptote. However, one shortcoming is the fact that there is no natural way to extrapolate such a function outside the data region at either small or large r. In particular, the fact that natural splines are used means that the resulting functions will always have zero curvature at the first and last grid points, and that some *ad hoc* procedure will have to be used to attach both a sensibly steep extrapolating function at the inner end of the data-sensitive region and the requisite inverse-power-sum tail at the outer end. This makes it difficult for fits using this model to yield accurate estimates of the length of the extrapolation to the dissociation limit, or to determine experimental values of long-range potential coefficients. Another concern is that a relatively large number of potential parameters (typically ~ 50 grid-point function values) is required to define a high quality potential, so that of order 100 many-digit numbers must be precisely transcribed by those wishing to use such a potential function. Moreover, while physically interesting parameters such as the equilibrium bond length r_e and well depth $\mathfrak{D}_e$ may be determined from such potential functions, they are not explicit parameters of the model, and hence it is difficult to obtain realistic estimates of their uncertainties.

For the reasons listed above, SPP function do not provide the best type of model to use for ordinary single-well potential functions. However, for potentials with double minima or 'shelf' behaviour they are an unparalleled success, since no other functional form can provide a smooth, flexible function that can handle the relatively abrupt changes of character associated with such cases [62, 63]. This form has also been used in successful DPF treatments of molecular states with a rotationless potential energy barrier [64]. Thus, in spite of shortcomings associated with their extrapolation behaviour, SPP potential functions will remain an essential component of a spectroscopist's toolkit for the foreseeable future.

Documented computer programs for using DPF fits to spectroscopic data to determine analytic potentials having any of the potential function forms described above are publicly available [61, 65].

6.3.3 Initial Trial Parameters for Direct Potential Fits

Vibration-rotation level energies and level energy differences are not linear functions of potential function parameters. Thus, DPF data analysis procedures are always based on non-linear least-squares fits, and they always require realistic initial trial values of the parameters defining the chosen potential function form. This is another situation in which the traditional data analysis methods described in § 6.2 prove to be of enduring value, since an RKR potential can always provide a good first-order estimate of the potential, and fitting the analytic potential form of interest to RKR points can give good estimates of the required initial trial parameter values. Preliminary potentials may also be obtained by *ab initio* methods, but they will be less accurate than RKR potentials, so the latter are preferred, when they are available.

Both polynomial and SPP potential functions are linear functions of the relevant expansion parameters, so fitting their forms to a preliminary set of RKR or *ab initio* turning points presents no problems. Moreover, the Morse-type algebraic structure of EMO and MLR potentials means that it is also a relatively straightforward matter to obtain preliminary estimates of their exponent expansion parameters β_i . For example, the MLR function of Eq. (6.55) may be rearranged to give

$$\beta(r) \cdot y_p^{\rm eq}(r) \;=\; -\;\ln\left\{ \frac{u_{\rm LR}(r_e)}{u_{\rm LR}(r)} \left(1 \pm \sqrt{\frac{V_{\rm MLR}(r) - V_{\rm MLR}(r_e)}{\mathfrak{D}_e}} \right) \right\} \quad . \tag{6.61}$$

Since Eq. (6.59) shows that $\beta_{\rm MLR}(r)$ is a linear function of the expansion parameters β_i , given some plausible initial estimates of r_e and $\mathfrak{D}_e$, that initial set of turning points defines the right-hand-side of Eq. (6.61), and one may use an ordinary linear least-squares fit to determine the desired trial β_i values. A similar rearrangement of the expression Eq. (6.52) defining an EMO potential yields an expression analogous to Eq. (6.61) for determining initial estimates of the exponent expansion coefficients for that case. Given such a set of trial exponent expansion parameters, it is a straightforward matter to perform a proper nonlinear least-squares fit to the desired potential form to the given turning points, a procedure that also could optimize the assumed values of r_e and $\mathfrak{D}_e$ and for an MLR potential, possibly also the leading C_m coefficient(s).

In addition to serving as a means of providing realistic initial trial parameters for DPF data analyses, fits of given sets of turning points to Eqs. (6.52) or (6.55) can serve as a very efficient means for presenting the results of *ab initio* calculations of potential energy functions. A computer program for performing turning-point fits of this type is available (with a manual) on the www [66].

6.4 Born-Oppenheimer Breakdown Effects

The discussion of § 6.3 focused on the problem of determining analytic potential energy functions that accurately explain all of the available discrete spectroscopic data for specified molecular states in terms of eigenvalues of the radial Schrödinger equation Eq. (6.1). For a heavy molecule such as Rb_2, a single potential energy function usually will suffice to explain the results for all isotopologues of that species. However, for species of small-reduced-mass, Born-Oppenheimer breakdown (BOB) effects give rise both to differences between the effective potentials for different isotopologues, and to atomic-mass-dependent corrections to the simple centrifugal potential $\left(\hbar^2/2\mu r^2\right)\,[J(J{+}1)]$ of Eq. (6.2). This has import with respect to the determination of equilibrium structures, since most observed transitions involve excited rotational levels, and it is the extrapolation of their properties to $J = 0$ that allows the determination of equilibrium structures and properties.

In practice, BOB effects often may be accounted for with ordinary DPF methodology simply by introducing atomic-mass-dependent terms into the effective potential energy function of Eq. (6.2). Most such work reported to date has been based on the effective radial Schrödinger equation derived by Watson [67, 68], in which atomic-mass-dependent non-adiabatic contributions to the kinetic energy operator are incorporated both into an effective 'adiabatic' contribution to the electronic potential energy function, and into the non-adiabatic BOB contribution to the effective centrifugal potential energy of the rotating molecule. Following the conventions of Refs. [69, 50], the resulting effective radial Schrödinger equation for isotopologue α of

molecule A–B in a singlet electronic state may be written as

$$\left\{ -\frac{\hbar^2}{2\mu_\alpha}\,\frac{d^2}{dr^2} \;+\; \left[V_{\rm ad}^{(1)}(r) \;+\; \Delta V_{\rm ad}^{(\alpha)}(r) \right] \right. \\ \left. +\; \frac{[J(J+1)]\hbar^2}{2\mu_\alpha\, r^2} \left[1 + g^{(\alpha)}(r) \right] \right\} \psi_{v,J}(r) \;=\; E_{v,J}\; \psi_{v,J}(r) \quad . \tag{6.62}$$

Here, $V_{\rm ad}^{(1)}(r)$ is the total electronic internuclear potential for a selected reference isotopologue (labeled $\alpha = 1$), $\Delta V_{\rm ad}^{(\alpha)}(r)$ is the *difference* between the effective adiabatic potentials for isotopologue–α and for the reference species ($\alpha = 1$), and $g^{(\alpha)}(r)$ is the non-adiabatic centrifugal potential correction function for isotopologue–α. Both $\Delta V_{\rm ad}^{(\alpha)}(r)$ and $g^{(\alpha)}(r)$ are written as sums of two terms, one for each component atom, whose magnitudes are inversely proportional to the mass of the particular atomic isotope [67, 68, 70, 69],

$$\Delta V_{\rm ad}^{(\alpha)}(r) \;=\; \frac{\Delta M_A^{(\alpha)}}{M_A^{(\alpha)}}\; \widetilde{S}_{\rm ad}^{A}(r) \;+\; \frac{\Delta M_B^{(\alpha)}}{M_B^{(\alpha)}}\; \widetilde{S}_{\rm ad}^{B}(r) \tag{6.63}$$

$$g^{(\alpha)}(r) \;=\; \frac{M_A^{(1)}}{M_A^{(\alpha)}}\; \widetilde{R}_{\rm na}^{A}(r) \;+\; \frac{M_B^{(1)}}{M_B^{(\alpha)}}\; \widetilde{R}_{\rm na}^{B}(r) \quad , \tag{6.64}$$

in which $\Delta M_A^{(\alpha)} = M_A^{(\alpha)} - M_A^{(1)}$ is the difference between the atomic mass of atom A in isotopologue α and in the reference isotopologue ($\alpha = 1$).

For a given isotopologue α, Eq. (6.62) effectively has the same form as Eq. (6.1), so the full machinery of DPF data analysis described in § 6.3 can be applied. The only difference is that in addition to the parameterized analytic potential energy function $V_{\rm ad}^{(1)}(r)$, the fit must simultaneously consider parameters defining the adiabatic and non-adiabatic radial strength functions $\widetilde{S}_{\rm ad}^{A/B}(r)$ and $\widetilde{R}_{\rm na}^{A/B}(r)$. This is a very straightforward matter, and raises no significant practical problems. Indeed, the fact that these contributions to the radial Hamiltonian are relatively small means that no effort need be devoted to obtaining initial trial values of the parameters defining these BOB radial strength functions. As a result, simultaneous fits to data sets for multiple isotopologues to determine both an analytic potential energy function and BOB radial strength functions have been 'routine' since the early 1990's [47].

As in the case of the potential energy function, some thought must be given to the analytic form of the radial strength functions $\widetilde{S}_{\rm ad}^{A/B}(r)$ and $\widetilde{R}_{\rm na}^{A/B}(r)$ [50]. For one thing, $\widetilde{S}_{\rm ad}^{A/B}(r)$ must have the same limiting long-range inverse-power behaviour as the potential function itself, since different isotopic forms of a given molecular species are normally[3] expected to have the same limiting long-range functional behaviour. A second point is that for an electronic state that dissociates to yield an atom in an excited electronic state, the limiting asymptotic value of $\widetilde{S}_{\rm ad}^{A/B}(r)$ must correlate with any difference in the associated atomic energy level spacing. For the case of a molecular state of species A–B which dissociates to yield both atoms in excited electronic states, $A^* + B^*$, the overall adiabatic correction to the potential for isotopologue–α must approach a limiting value equal to the sum of the associated atomic isotope shifts:

$$\lim_{r\to\infty} \Delta V_{\rm ad}^{(\alpha)}(r) \;=\; \delta E^{(\alpha)}(A^*) + \delta E^{(\alpha)}(B^*) \quad , \tag{6.65}$$

in which $\delta E^{(\alpha)}(A^*)$ is the difference between the $A \to A^*$ atomic excitation energy of the isotope of that atom in molecular isotologue α *vs.* the corresponding value for the reference isotopologue. Note that this expression assumes that the absolute zero of energy for a given molecular species is set at the limit for dissociation to two ground state atoms; analogous (but more complicated) constraints would arise for other choices of the reference energy.

The above constraints on the adiabatic radial strength functions $\widetilde{S}_{\rm ad}^{A/B}(r)$ are taken into account by the same type of analytic form used for the MLR potential exponent coefficient:

$$\widetilde{S}_{\rm ad}^{A}(r) \;=\; y_{p_{\rm ad}}^{\rm eq}(r)\; u_\infty^A \;+\; [1 - y_{p_{\rm ad}}^{\rm eq}(r)] \sum_{i=0} u_i^A \left(y_{q_{\rm ad}}^{\rm eq}(r) \right)^i \quad , \tag{6.66}$$

[3] An example of a special exception to this rule is the $A\,^3\Sigma_u^+$ state of $^{6,7}Li_2$ discussed in Ref. [53].

in which $p_{\rm ad}=m_1$, the power of the leading inverse-power term in the long-range potential for the state in question, and u_∞^A is defined as

$$u_\infty^A \;=\; \delta E^{(\alpha)}(A^*)\;\left(M_A^{(\alpha)}/\Delta M_A^{(\alpha)}\right) \quad . \tag{6.67}$$

There is no physical constraint on the value of the the integer $q_{\rm ad}$ defining the power series expansion variable in Eq. (6.66), but experience shows that it should be larger that 1 (say $q_{\rm ad}\gtrsim 3$) to prevent the resulting function from having implausible extrema in the interval between the data region and the asymptotic limit [50]. If the associated radial expansion variables are expressed relative to r_e (i.e., solely in terms of $y_{p/q}^{\rm eq}(r)$), this form also allows the difference in isotopic dissociation energies to be written as

$$\delta\mathfrak{D}_e^{(\alpha)} \;=\; \mathfrak{D}_e^{(\alpha)}-\mathfrak{D}_e^{(1)} \;=\; \frac{\Delta M_A^{(\alpha)}}{M_A^{(\alpha)}}\;(u_\infty^A-u_0^A) \;+\; \frac{\Delta M_B^{(\alpha)}}{M_B^{(\alpha)}}\;(u_\infty^B-u_0^B) \quad . \tag{6.68}$$

Most of the considerations discussed above also apply to the non-adiabatic centrifugal radial strength functions $\widetilde{R}_{\rm ad}^{A/B}(r)$, so the same type of analytic form may be used to represent these functions:

$$\widetilde{R}_{\rm na}^{A}(r) \;=\; y_{p_{\rm na}}^{\rm eq}(r)\;t_\infty^A \;+\; [1-y_{p_{\rm na}}^{\rm eq}(r)]\;\sum_{i=1}\;t_i^A\left(y_{p_{\rm na}}^{\rm eq}(r)\right)^i \quad . \tag{6.69}$$

In this case, however, there is no constraint on the limiting long-range form of the function, so there is no point in using different powers to define the radial variables in the summation and in the other two y_p-factors. Moreover, physical arguments indicate that for neutral molecules $t_\infty^{A/B}=0$, while for a molecular ion which dissociates to yield (say) $A^{+Q}+B$, it is defined in terms of Watson's 'charge-modified reduced mass' [67] and the conventional reduced mass of the dissociation products [50]. Note that the power-series summation in Eq. (6.69) has no constant term because the derivation of Eq. (6.62) gave rise to an indeterminacy which is best accounted for by assuming that $g^{(\alpha)}(r=r_e)=0$ [67, 68].

The constraint that $g^{(\alpha)}(r_e)=0$ (i.e., that $t_0^{A/B}=0$) means the isotopologue dependence of the equilibrium bond length is defined by the value of the first radial derivative of the adiabatic correction function $\Delta V_{\rm ad}^{(\alpha)}(r)$ at $r=r_e$. In terms of the parameterization presented above this means that

$$\delta r_e^{(\alpha)} \;=\; r_e^{(\alpha)}-r_e^{(1)} \;=\; \frac{\Delta M_A^{(\alpha)}}{M_A^{(\alpha)}}\;\frac{\widetilde{S}_{\rm ad}^A(r_e)'}{\tilde{k}} \;+\; \frac{\Delta M_B^{(\alpha)}}{M_B^{(\alpha)}}\;\frac{\widetilde{S}_{\rm ad}^B(r_e)'}{\tilde{k}} \quad , \tag{6.70}$$

in which $\tilde{k}$ is the harmonic force constant of the potential function at its minimum and the radial derivative of $\widetilde{S}_{\rm ad}^A(r_e)$ ma be written as

$$\widetilde{S}_{\rm ad}^A(r_e)' \;\equiv\; \left(\frac{d\widetilde{S}_{\rm ad}^A(r)}{dr}\right)_{r=r_e} \;=\; \frac{(u_\infty^A-u_0^A)\,p_{\rm ad}^A+u_1^A\;q_{\rm ad}^A}{2\,r_e} \quad . \tag{6.71}$$

Finally, we note that straightforward extensions of Eq. (6.62) have also been developed that take account of the *e/f* Λ-doubling splittings which occurs for singlet states with non-zero integer electronic orbital angular momentum [51], and for the spin splittings of rotational levels in $^2\Sigma$ states [65, 56]. Treatments of all of these BOB effects are incorporated into the publicly available DPF data analysis program `DPotFit` [65].

6.5 Concluding Remarks

This chapter has shown that the analysis of diatomic molecule spectroscopic data can yield both very accurate equilibrium properties, including bond lengths and well depths, and accurate overall potential energy functions. The accuracy of bond lengths determined in this way will match that of experimental B_v values for the lowest observed vibrational levels, with typical uncertainties of order $10^{-4}-10^{-6}$ Å, while the uncertainties in the associated dissociation energies are no more than a few % of the binding energy of the highest observed vibrational level.

The standard methods described herein often also allow accurate resolution of isotopic differences, both in equilibrium parameters and in the overall potential energy curves, due to Born-Oppenheimer breakdown. However, one cautionary note must be raised regarding the isotopologue dependence of equilibrium bond lengths. The discussion of § 6.4 attributes all such effects to the slope and curvature of the effective adiabatic correction potential $\Delta V_{\rm ad}^{(\alpha)}(r)$ appearing in Eq. (6.62), because the Watson convention [67, 68] of defining the equilibrium value of the non-adiabatic centrifugal potential correction function $g^{(\alpha)}(r_e)$ to be precisely zero has been adopted. As was pointed out in Ref. [67], this is an *ad hoc* assumption introduced because of a fundamental indeterminacy associated with removal of the atomic-mass-dependent non-adiabatic contribution to the kinetic energy operator in order to obtain the working Hamiltonian of Eq. (6.62). Unfortunately, it is impossible to improve on this description using only the information contained in transition energies, and since the effects of this approximation may be expected to be very small, it suffices for almost all practical purposes.

Traditional "parameter-fit" analyses of experimental data based on equations such as (6.4) and (6.16) have been shown to be at least partially superceded by the DPF methods of § 6.3. However, both the traditional methods and the associated semiclassical methods of § 6.2 remain of enduring value, both because of the physical insight they offer, and because of their practical importance in providing the realistic initial trial parameters required by DPF methods. Within the DPF methodology, it is also clear that use of an appropriate analytic potential energy functional form is of central importance for obtaining an optimally compact, flexible, and accurate potential energy function that extrapolates realistically at both large and small distances. Three keys to these objectives are: (i) placing most of the flexibility of the potential energy function in a parameterized exponent coefficient, rather than in linear terms, (ii) choosing an optimal definition for the radial expansion variable, and (iii) incorporating the theoretically-known limiting long-range behaviour within the overall functional form, rather than having it as a separate attached tail.

While the present discussion has been focussed on diatomic molecules, the DPF method was originally introduced as a way of describing three-dimensional atom-diatom systems [41]. The type of potential energy function description used herein has already proved useful for atom-molecule and molecule-molecule Van der Waals systems [71, 72], and in due course this type of approach can be expected to be applied to more 'normal' polyatomic molecules.

Appendix. What Terms Contribute to a Long-Range Potential?

If two atoms lie sufficiently far apart that their electron clouds overlap negligibly, then their interaction energy may be expanded as the simple inverse-power sum of Eq. (6.33). The nature of the atomic species to which a given molecular state dissociates determines which powers contribute to this sum. More complete discussion may be found in Refs. [73, 74, 75, 76].

An $m = 1$ term will arise in Eq. (6.33) only for ion-pair states that dissociate to yield two atoms with permanent charges. In this case the interaction coefficient is $C_1 = -Z_a\, Z_b\, e^2/4\pi\epsilon_0$, in which Z_a and Z_a are the ($\pm$ integer) number of charges on atoms a and b, respectively.

An $m=2$ term arises classically from the interaction between a permanent charge and a permanent dipole moment. Although no atom possesses a permanent dipole moment, an electronically excited one-electron atom such as excited H or He^+ may behave as if it does, since the presence of the interaction partner can cause a mixing of degenerate states of different symmetry to yield a hybrid atomic orbital which is effectively dipolar. If its interaction partner is an ion, it will contribute an $m = 2$ term to Eq. (6.33).

An $m = 3$ term arises classically from the interaction between two permanent dipole moments. The preceding discussion indicates that this could occur in the interaction of two electronically excited one-electron atoms, each of which is in a dipolar hybrid state. However, a much broader range of cases involves the interaction between a pair of atoms of the same species in different atomic states between which electric dipole transitions are allowed. In this case, the 'resonance' mixing of the wavefunctions for two equivalent atoms whose total orbital angular momentum quantum numbers differ by one (i.e., S with P, or P with D) effectively makes them act as if they both had permanent dipole moments, and an r^{-3} interaction energy arises.

Another type of r^{-3} term can arise from the first-order interaction between an ion and a particle with a permanent quadrupole moment (e.g., with a P–state atom). For this case $C_3 \propto Z_a\, e\, Q_b$, where $Z_a\, e$ is the charge on the ion and Q_b is the permanent quadrupole moment on its interaction partner.

An $m=4$ term could arise in first order from the interaction of an ion with a particle having a permanent octupole moment (e.g., a D–state atom), or between a particle with (or acting as if it had) a permanent dipole moment and a species having a permanent quadrupole moment. In both cases the associated C_4 interaction coefficients would be proportional to the product of the two charge moments with a factor defined by the symmetry of the particular molecular state.

A more common type of r^{-4} interaction term arises as the second-order charge-induced dipole interaction between an ion and the electron distribution of its interaction partner. For this case $C_4 = \left({Z_a}^2\, e^2/4\pi\epsilon_0\right)\, \alpha_{\rm d}^b/2$, in which $Z_a\, e$ is the charge on the ion (atom–a) and $\alpha_{\rm d}^b$ the dipole polarizability of particle–b. This is usually the leading long-range term for molecular ions.

An $m=5$ term arises from the classical electrostatic interaction of two permanent quadrupole moments. Thus, it will contribute to the long-range potential whenever *neither* of the interacting atoms is in an S state. As with all first-order interactions, the associated C_5 coefficient is proportional to the product of the associated permanent moments with a factor depending on the symmetry of the particular molecular state, or more particularly, as the product of an electronic state symmetry factor times $\langle {r_e}^2\rangle_a\, \langle {r_e}^2\rangle_b$, where $\langle {r_e}^2\rangle_\alpha$ is the expectation value of square of the electron radius in the unfilled valence shell of atom–α.

"Dispersion energy" terms with $m = 6,\ 8,\ 10,\ \ldots$ etc., arise in second-order perturbation theory and contribute to *all* interactions between atomic particles (except when one is a bare nucleus). For the case of uncharged atoms, at least one of which is in an S–state, these are the leading (longest-range) contributions to Eq. (6.33). Because they arise in second-order perturbation theory, these terms are always attractive for pairs of ground-state atoms.

Acknowledgements

I am very grateful to Professor F.R.W. McCourt for his detailed, constructive comments on the manuscript.

Exercises

1. Making use of the fact that the semiclassical value for the expectation value of the property $f(r)$ is
$$\langle f(r)\rangle \;=\; \int_0^\infty \frac{f(r)\,dr}{[G_v - V(r)]^{1/2}} \Big/ \int_0^\infty \frac{dr}{[G_v - V(r)]^{1/2}} \quad , \tag{6.72}$$
use the machinery of § 6.2.3 to determine an explicit near-dissociation theory expression for the expectation value of $f(r)=r^2$.
2. For a potential whose long-range tail has the form $V(r) \simeq \mathfrak{D} - A\, e^{-br}$, derive the analog of Eq. (6.37).
3. Show that a polynomial potential expanded in terms of the Šurkus variable of Eq. (6.51) with $p=4$ cannot give a $1/r^6$ term.
4. Derive the 'geometric mean rule' for $r_{\rm ref}$ which was presented in the second-last paragraph of § 6.3.2 B.
5. From consideration of the limiting long-range behaviour of Eq. (6.59), show why it is necessary to set $p > (m_{\rm last} - m_{\rm first})$ in the definition of an MLR potential.
6. Determine the limiting long-range behaviour of Eq. (6.66), and show that it is $\propto r^{-m_1}$
7. What is the limiting *short-range* functional behaviour of an MLR potential energy function? (A simple way of removing this high-order singularity has been devised.)

Bibliography

[1] Le Roy, R. J.; Bernstein, R. B. *J. Chem. Phys.* **1971**, *54*, 5114-5126.

[2] Le Roy, R. J.; Liu, W.-K. *J. Chem. Phys.* **1978**, *69*, 3622-3631.

[3] Le Roy, R. J. LEVEL 8.0: *A Computer Program for Solving the Radial Schrödinger Equation for Bound and Quasibound Levels*, University of Waterloo Chemical Physics Research Report CP-663; see http://leroy.uwaterloo.ca/programs/, 2007.

[4] Cooley, J. W. *Math. Computations* **1961**, *15*, 363-374.

[5] Herzberg, G. *Spectra of Diatomic Molecules*; Van Nostrand: New York, 1950.

[6] a) Hutson, J. M. *J. Phys. B. (At. Mol. Phys.)* **1981**, *14*, 851–857; b) Hutson, J. M. *QCPE Bulletin*, *2*, no. 2, Program #435, Quantum Chemistry Program Exchange, Indiana University, Bloomington, Indiana, 1981.

[7] Tellinghuisen, J. *J. Mol. Spectrosc.* **1987**, *122*, 455-461.

[8] Kilpatrick, J. E.; Kilpatrick, M. F. *J. Chem. Phys.* **1951**, *19*, 930-933.

[9] Kilpatrick, J. E. *J. Chem. Phys.* **1959**, *30*, 801-805.

[10] Child, M. S. *Semiclassical Methods in Molecular Scattering and Spectroscopy*; D. Reidel: Dordrecht, 1980.

[11] Child, M. S. *Semiclassical Mechanics with Molecular Applications*; Clarendon Press: Oxford, 1991.

[12] Abramowitz M.; Stegun, I. A. *Handbook of Mathematical Functions*; Dover: New York, 1970.

[13] a) Dunham, J. L. *Phys. Rev.* **1932**, *41*, 713-770; b) Dunham, J. L. *Phys. Rev.* **1932**, **41**, 721-731.

[14] Fröman, N. 1980. In *Semiclassical Methods in Molecular Scattering and Spectroscopy*, Child, M. S., Ed.; Series C - Mathematical and Physical Sciences; Riedel: Dordrecht, 1980, Vol. 53, 1-44.

[15] Kirschner, S. M.; Le Roy, R. J. *J. Chem. Phys.* **1978**, *68*, 3139-3148.

[16] Paulsson, R.; Karlsson, F.; Le Roy, R. J. *J. Chem. Phys.* **1983**, *79*, 4346-4354.

[17] Schwartz C.; Le Roy, R. J. *J. Mol. Spectrosc.* **1987**, *121*, 420-439.

[18] Oldenberg, O. *Z. Physik* **1929**, *56*, 563-575.

[19] Rydberg, R. *Z. Physik* **1931**, *73*, 376-385.

[20] Klein, O. *Z. Physik* **1932**, *76*, 226-235.

[21] Rees, A. L. G. *Proc. Phys. Soc. (London)* **1947**, *59*, 998-1008.

[22] Dickinson, A. S. *J. Mol. Spectrosc.* **1972**, *44*, 183-188.

[23] Fleming H. E.; Rao, K. N. *J. Mol. Spectrosc.* **1972**, *44*, 189-193.

[24] Tellinghuisen, J. *J. Mol. Spectrosc.* **1972**, *44*, 194-196.

[25] Verma, R. D. *J. Chem. Phys.* **1960**, *32*, 738-749.

[26] Tellinghuisen, J.; Henderson, S. D. *Chem. Phys. Lett.* **1982**, *91*, 447-451.

[27] Le Roy, R. J. RKR1 2.0: *A Computer Program Implementing the First-Order RKR Method for Determining Diatomic Molecule Potential Energy Curves*, University of Waterloo Chemical Physics Research Report CP-657; see http://leroy.uwaterloo.ca/programs/, 2003.

[28] Kaiser, E. W. *J. Chem. Phys.* **1970**, *53*, 1686-1703.

[29] Birge R. T.; Sponer, H. *Phys. Rev.* **1926**, *28*, 259-283.

[30] a) Le Roy, R. J.; Bernstein, R. B. *Chem. Phys. Lett.* **1970**, *5*, 42; b) Le Roy, R. J.; R. B. Bernstein. *J. Chem. Phys.* **1970**, *52*, 3869-3879.

[31] Le Roy, R. J. In *Semiclassical Methods in Molecular Scattering and Spectroscopy*, Child, M. S., Ed.; Series C - Mathematical and Physical Sciences; Riedel: Dordrecht, 1980, Vol. 53, 109–126.

[32] Le Roy, R. J. *Can. J. Phys.* **1972**, *50*, 953-959.

[33] Tanaka, Y.; Yoshino, K. *J. Chem. Phys.* **1970**, *53*, 2012-2030.

[34] Le Roy, R. J. *J. Chem. Phys.* **1972**, *57*, 573-574.

[35] Takasu, Y.; Komori, K.; Honda, K.; Kumakura, M.; Yabuzaki, T. and Takahashi, Y. *Phys. Rev. Lett.* **2004**, *93*, 123202/1-4.

[36] Le Roy, R. J. *J. Chem. Phys.* **1980**, *73*, 6003-6012.

[37] Le Roy, R. J. *J. Chem. Phys.* **1994**, *101*, 10217-10228.

[38] Tellinghuisen. J.; Ashmore, J. G. *Chem. Phys. Lett.* **1983**, *102*, 10-16.

[39] Ashmore, J. G.; Tellinghuisen, J. *J. Mol. Spectrosc.* **1986**, *119*, 68-82.

[40] Le Roy, R. J. DParFit 3.3: *A Computer Program for Fitting Multi-Isotopologue Diatomic Molecule Spectra*, University of Waterloo Chemical Physics Research Report CP-660; see http://leroy.uwaterloo.ca/programs/, 2005

[41] Le Roy, R. J.; van Kranendonk, J. *J. Chem. Phys.* **1974**, *61*, 4750-4769.

[42] Ogilvie, J. F. *Proc. Roy. Soc.* (London) **1981**, *A 378*, 287-300.

[43] Ogilvie, J. F. *J. Chem. Phys.* **1988**, *88*, 2804-2808.

[44] Šurkus, A. A.; Rakauskas, R. J.; Bolotin, A. B. *Chem. Phys. Lett.* **1984**, *105*, 291-294.

[45] Samuelis, C.; Tiesinga, E.; Laue, T.; Elbs, M.; Knöckel, H.; Tiemann, E. *Phys. Rev. A* **2000**, *63*, 012710/1-11.

[46] Coxon, J. A.; Hajigeorgiou, P. G. *J. Mol. Spectrosc.* **1990**, *139*, 84-106.

[47] Coxon, J. A.; Hajigeorgiou, P. G. *J. Mol. Spectrosc.* **1991**, *150*, 1-27.

[48] Coxon, J. A.; Hajigeorgiou, P. G. *Can. J. Phys.* **1992**, *70*, 40-54.

[49] Hajigeorgiou, P. G.; Le Roy, R. J. *J. Chem. Phys.* **2000**, *112*, 3949-3957.

[50] Le Roy, R. J.; Huang, Y. *J. Mol. Struct.* (Theochem) **2002**, *591*, 175-187.

[51] Huang, Y.; Le Roy, R. J. *J. Chem. Phys.* **2003** *119*, 7398-7416; erratum *ibid* **2007**, *126*, 169904/1-1.

[52] Le Roy, R. J.; Appadoo, D. R. T.; Anderson, K.; Shayesteh, A.; Gordon, I. E.; Bernath, P. F. *J. Chem. Phys.* **2005**, *123*, 204304/1-12.

[53] Le Roy, R. J.; Dattani, N.; Coxon, J. A.; Ross, A. J.; Crozet, P.; Linton, C. *J. Chem. Phys.* **2009**, *131*, 204309/1-17.

[54] Le Roy, R. J.; Tao, J.; Haugen, C.; Henderson, R. D. E.; Wu, Y.-R. 2010. unpublished work.

[55] Le Roy, R. J.; Henderson, R. D. E. *Mol. Phys.* **2007**, *105*, 663-677.

[56] Shayesteh, A.; Henderson, R. D. E.; Le Roy, R. J.; Bernath, P. F. *J. Phys. Chem. A* **2007**, *111*, 12495-12505.

[57] Tiemann, E. *Z. Phys. D – Atoms, Molecules and Clusters* **1987**, *5*, 77-82.

[58] Wolf, U.; Tiemann, E. *Chem. Phys. Lett.* **1987**, *133*, 116-120.

[59] Wolf, U.; Tiemann, E. *Chem. Phys. Lett.* **1987**, *139*, 191-195.

[60] Tiemann, E. *Mol. Phys.* **1988**, *65*, 359-375.

[61] Pashov, A.; Jastrzębski, W.; Kowalczyk, P. *Comp. Phys. Comm.* **2000**, *128*, 622-634.

[62] Pashov, A.; Jastrzębski, W.; Kowalczyk, P. *J. Chem. Phys.* **2000**, *113*, 6624-6628.

[63] Pashov, A.; Jastrzębski, W.; Jaśniecki, W.; Bednarska, V.; Kowalczyk, P. *J. Mol. Spectrosc.* **2000**, *203*, 264-267.

[64] Bouloufa, N.; Cacciani, P.; Vetter, R.; Yiannopoulou, A.; Martin, F.; Ross, A. J. *J. Chem. Phys.* **2001**, *114*, 8445-8458.

[65] Le Roy, R. J.; Seto, J.; Huang, Y. DPotFit 1.2: *A Computer Program for fitting Diatomic Molecule Spectra to Potential Energy Functions*, University of Waterloo Chemical Physics Research Report CP-664; see http://leroy.uwaterloo.ca/programs/, 2007.

[66] Le Roy, R. J. betaFIT 2.0: *A Computer Program to Fit Potential Function Points to Selected Analytic Functions*, University of Waterloo Chemical Physics Research Report CP-665; see http://leroy.uwaterloo.ca/programs/, 2009.

[67] Watson, J. K. G. *J. Mol. Spectrosc.* **1980**, *80*, 411-421.

[68] Watson, J. K. G. *J. Mol. Spectrosc.* **2004**, *223*, 39-50.

[69] Le Roy, R. J. *J. Mol. Spectrosc.* **1999**, *194*, 189-196.

[70] Ogilvie, J. F. *J. Phys. B: At. Mol. Opt. Phys.* **1994**, *27*, 47-61.

[71] Li, H.; Le Roy, R. J. *Phys. Chem. Chem. Phys.* **2008**, *10*, 4128-4137.

[72] Li, H.; Roy, P.-N.; Le Roy, R. J. *J. Chem. Phys.* **2010**, *132*, 214309/1–14.

[73] Margenau, H. *Rev. Mod. Phys.* **1939**, *11*, 1-35.

[74] Hirschfelder, J. O.; Curtiss, C. F.; Bird, R. B. *Molecular Theory of Gases and Liquids*; Wiley: New York, 1964.

[75] Hirschfelder, J. O.; Meath, W. J. In *Intermolecular Forces*, Hirschfelder, J. O., Ed.; *Adv. Chem. Phys.*; Interscience: New York, 1967; 12, 3–106

[76] Maitland, G. C.; Rigby, M.; Smith, E. B.; Wakeham, W. A. *Intermolecular Forces - Their Origin and Determination*; Oxford University Press: Oxford, 1981.